Human Molecular Genetics, 2015, Vol. 24, No. 7 1956–1976

doi: 10.1093/hmg/ddu611
Advance Access Publication Date: 8 December 2014
Original Article

ORIGINAL ARTICLE

Biochemical and cellular analysis of Ogden syndrome reveals downstream Nt-acetylation defects

Line M. Myklebust[1,†], Petra Van Damme[2,3,†,*], Svein I. Støve[1,4,†], Max J. Dörfel[5,†], Angèle Abboud[1,6], Thomas V. Kalvik[1], Cedric Grauffel[1,6], Veronique Jonckheere[2,3], Yiyang Wu[5,7], Jeffrey Swensen[8], Hanna Kaasa[1], Glen Liszczak[9,10,11], Ronen Marmorstein[9,10,11], Nathalie Reuter[1,6], Gholson J. Lyon[5,7,*], Kris Gevaert[2,3] and Thomas Arnesen[1,4,*]

[1]Department of Molecular Biology, University of Bergen, Bergen N-5020, Norway, [2]Department of Medical Protein Research, VIB, B-9000 Ghent, Belgium, [3]Department of Biochemistry, Ghent University, B-9000 Ghent, Belgium, [4]Department of Surgery, Haukeland University Hospital, N-5021 Bergen, Norway, [5]Stanley Institute for Cognitive Genomics, Cold Spring Harbor Laboratory, Woodbury, NY 11797, USA, [6]Computational Biology Unit, Uni Computing, Uni Research AS, Bergen, Norway, [7]Department of Molecular Genetics and Microbiology, Stony Brook University, Stony Brook, NY 11794, USA, [8]Caris Life Sciences, Phoenix, AZ, USA, [9]Program in Gene Expression and Regulation, Wistar Institute, PA 19104, USA, [10]Department of Chemistry, and [11]Department of Biochemistry and Biophysics and Abramson Family Cancer Research Institute, Perelman School of Medicine, University of Pennsylvania, Philadelphia, PA 19104, USA

*To whom correspondence should be addressed at: Department of Molecular Biology, University of Bergen, N-5020 Bergen, Norway. Tel: +47 55584528; Fax: +47 55589683; Email: Thomas.Arnesen@mbi.uib.no (T.A.); Department of Medical Protein Research, Flanders Interuniversity Institute for Biotechnology, Ghent University, A. Baertsoenkaai 3, B-9000 Ghent, Belgium. Tel: +32 92649279; Fax: +32 92649496; Email: Petra.vandamme@vib-ugent.be (P.V.D.); Stanley Institute for Cognitive Genomics, Cold Spring Harbor Laboratory, Woodbury, NY 11797, USA. Tel: +1 6468721219; Fax: +1 5164224109; Email: gholsonjlyon@gmail.com (G.J.L.)

Abstract

The X-linked lethal Ogden syndrome was the first reported human genetic disorder associated with a mutation in an N-terminal acetyltransferase (NAT) gene. The affected males harbor an Ser37Pro (S37P) mutation in the gene encoding Naa10, the catalytic subunit of NatA, the major human NAT involved in the co-translational acetylation of proteins. Structural models and molecular dynamics simulations of the human NatA and its S37P mutant highlight differences in regions involved in catalysis and at the interface between Naa10 and the auxiliary subunit hNaa15. Biochemical data further demonstrate a reduced catalytic capacity and an impaired interaction between hNaa10 S37P and Naa15 as well as Naa50 (NatE), another interactor of the NatA complex. N-Terminal acetylome analyses revealed a decreased acetylation of a subset of NatA and NatE substrates in Ogden syndrome cells, supporting the genetic findings and our hypothesis regarding reduced Nt-acetylation of a subset of NatA/NatE-type substrates as one etiology for Ogden syndrome. Furthermore, Ogden syndrome fibroblasts display abnormal cell migration

[†]These authors contributed equally to this work.

Received: October 16, 2014. **Revised and Accepted:** December 3, 2014

and proliferation capacity, possibly linked to a perturbed retinoblastoma pathway. N-Terminal acetylation clearly plays a role in Ogden syndrome, thus revealing the *in vivo* importance of N-terminal acetylation in human physiology and disease.

Introduction

Protein acetylation is one of the most common protein modifications occurring both on lysine side chains in proteins and at protein N termini (1). Nt-acetylation is mainly co-translational and presumed to be an irreversible covalent modification catalyzed by the ribosome associated N-terminal acetyltransferases (NATs), members of the Gcn5-related *N*-acetyltransferase superfamily of acetyltransferases (2). NATs transfer an acetyl moiety from acetyl coenzyme A (Ac-CoA) to the primary α-amino group of nascent polypeptides as they emerge from ribosomes, and proteomic analyses have revealed that 50–90% of yeast, plant, fruit fly and human proteins are Nt-acetylated (1,3–5).

Originally, Nt-acetylation was assumed to protect proteins from degradation (6). However, current findings link Nt-acetylation to degradation of some proteins, via Ac/N-degron-mediated recruitment of specific ubiquitin ligases (7,8). Nt-acetylation may also influence protein complex formation, as exemplified by the NEDD8 ligation enzymes (9), next to prion formation (10). Also, protein-specific targeting to membranes of the nucleus (11), Golgi (12,13) and lysosomes (14) was shown to require Nt-acetylation, but a general role in targeting is not supported (15). Some proteins destined for translocation through the endoplasmic reticulum are Nt-free, suggesting that Nt-acetylation of this pool of proteins inhibits translocation (16).

To date, six NATs (NatA–NatF) have been identified in higher eukaryotes and their substrate specificities have been characterized (2,17). Each NAT acetylates defined subsets of substrates mainly based on the identity of the first two amino acid residues of the nascent polypeptide (2), although there is some potential redundancy in the system with some NATs acetylating the same type of substrates. NatA, the major eukaryotic NAT in terms of targeted substrates, displays a broad substrate specificity profile by Nt-acetylating Ser-, Thr-, Ala-, Val-, Gly- and Cys-starting N termini of which the initiator methionine (iMet) was removed by the action of methionine aminopeptidase (1,18,19). The NatA complex is composed of the catalytic subunit, Naa10 (ARD1) and the auxiliary subunit Naa15 (NAT1/NATH) (19–21), which anchors Naa10 to the ribosome and modulates its catalytic activity (22,23). Furthermore, the catalytic subunit Naa50 (NAT5) defined as NatE (22,24) and in multicellular eukaryotes, the Huntingtin-interacting protein K (25) are physically associated with the NatA complex, but whether Naa50 exerts activity *in vivo* in a monomeric form or whether the active form of Naa50 is entirely dependent on its association with NatA (26–28) is still not known. Recently, the structures of the first eukaryotic NATs, human Naa50 and the *Schizosaccharomyces pombe* Naa10–Naa15 (NatA) complex, were elucidated by X-ray crystallography (23,29). These structures reveal the molecular mechanism and the key residues involved in substrate-specific Nt-acetylation. Besides co-translational Nt-acetylation by the NatA complex, it has been shown *in vitro* that monomeric Naa10 also displays posttranslational Nt-acetylation (28) and *in vitro* and *in vivo* (co- and/or post-translational) Nt-propionylation activity (30).

NatA function is not essential in yeast, but *Saccharomyces cerevisiae naa10Δ* and *naa15Δ* strains show defects in mating, sporulation, entry into stationary phase and temperature, salt and drug sensitivity (1,19,31). Loss of the *Drosophila melanogaster* Naa10 homolog results in lethality (32) as does loss of the corresponding homologs in *Trypanosoma brucei* (33) and *Caenorhabditis elegans* (34). Further, deregulated human Naa10 or NatA expression is linked to tumor development or progression, and depletion of NatA subunits from cancer cells induces cell cycle arrest or apoptosis (35).

In 2011, the first human genetic disorder, named Ogden syndrome, involving an Ser37Pro (S37P) mutation in hNaa10 was revealed (OMIM 300013) (36). This X-linked disorder is characterized by severe global developmental delays, comprising a unique combination of craniofacial anomalies, hypotonia, cardiac arrhythmia and eventual cardiomyopathy, resulting in mortality during infancy. Recently, the S37P mutant was shown to display reduced catalytic activity and a reduced ability to form a NatA complex when co-expressed with hNaa15 in yeast (37). A recent study also suggested the association of *de novo* putative frameshift mutations in h*NAA15* with congenital heart defects, consistent with the range of minor cardiac anomalies seen in Ogden syndrome (38). An h*NAA10* mutation resulting in expression of a truncated Naa10 protein was found in a single family with Lenz microphthalmia syndrome, however, showing very little overlap with the Ogden syndrome phenotype (39). Further, *de novo* missense mutations in h*NAA10* were identified and suggested to be involved in two unrelated individuals with global developmental delays (40).

We hypothesize that the hemizygous hypomorphic mutation in male infants with Ogden syndrome leads to decreased Nt-acetylation of key substrates important for the control and regulation of physiological processes dysregulated in Ogden syndrome. Here, we present the first evidence showing that impaired NatA-S37P complex formation and catalytic capacity of the human proteins leads to reduced *in vivo* Nt-acetylation of a subset of proteins in cells from an Ogden syndrome family.

Results

The hNaa10-S37P mutation affects the structure and dynamics of a human NatA structural model

In order to investigate the structural effects of the Ogden syndrome hNaa10-S37P mutation, we generated and simulated structural models of both the wild-type human NatA complex and the S37P mutant. Homology models were built based on the recently determined crystal structure of the NatA complex from *S. pombe* (23). As calculated by BLAST, the human and *S. pombe* Naa15 sequences share 39% identity and 57% similarity, and the human and *S. pombe* Naa10 sequences share 66% identity and 81% similarity (Supplementary Material, Fig. S1). Further, both mutant and WT NatA models complexed with Ac-CoA were each subjected to two independent 100 ns-long molecular dynamics (MD) simulations (Supplementary Material, Fig. S2). The resulting model of the WT complex is shown in Figure 1A–C. We observed that the S37P mutation shortens helix α2 of hNaa10 (Fig. 1D).

Similarly to what has been observed in the *S. pombe* complex (23), interactions between subunits of the human complex involve numerous hydrophobic contacts via helices α1 and α2 of hNaa10 and helices 25, 27, 28, 29 and 30 of hNaa15 (Fig. 1C). Free energy decomposition analysis using the molecular mechanics (MM)/Poisson Boltzman surface area (PBSA) scheme shows that these amino acids contribute significantly to the

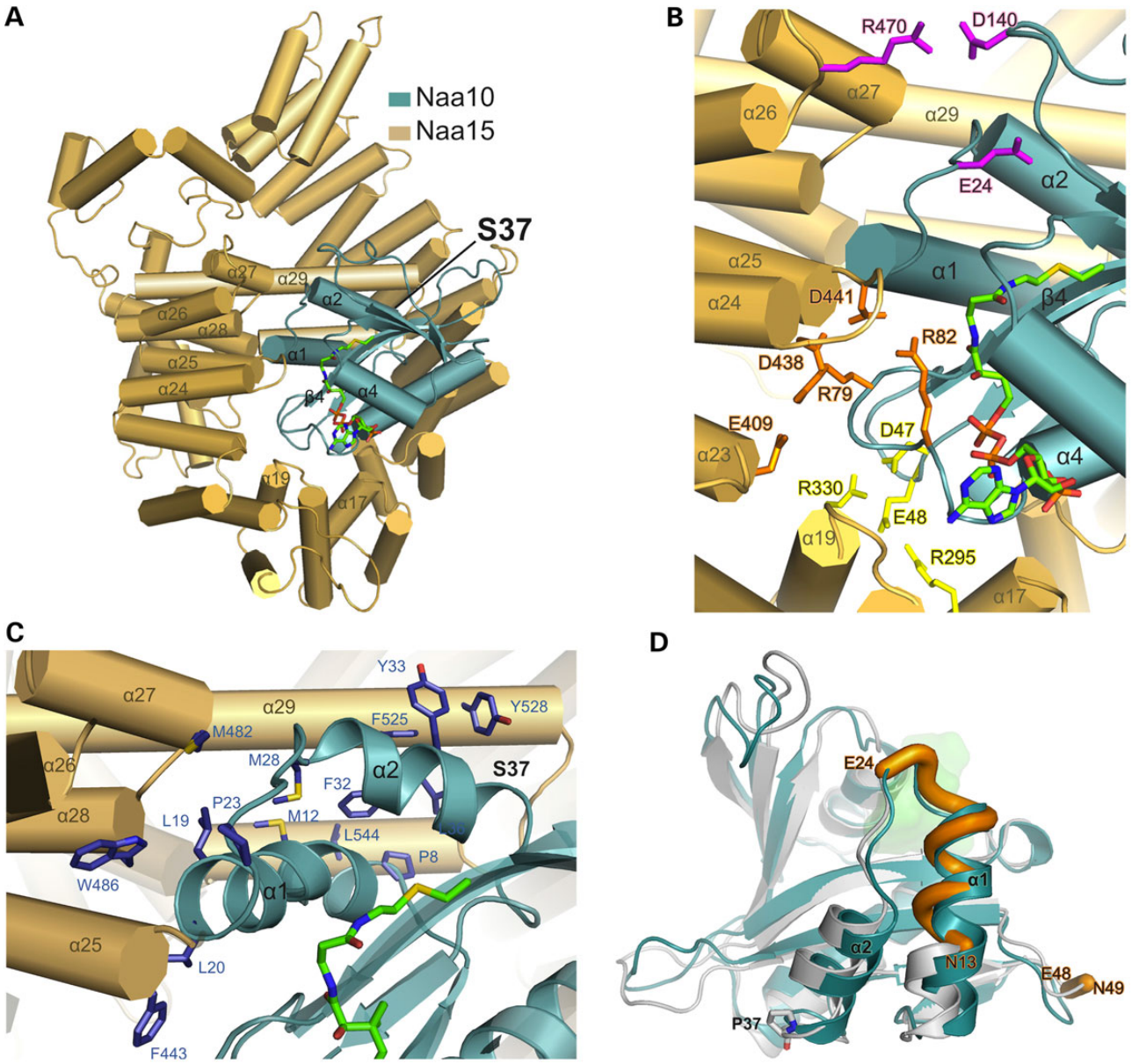

Figure 1. 3D structural models of the human WT and S37P Naa10–Naa15 complex. (**A**) WT NatA complex containing Naa15 (brown cartoons) and Naa10 (cyan cartoons) after 100 ns MD simulations. Only helices involved in the most relevant interactions between Naa15 and Naa10 are labeled. A black arrow indicates the mutation point, serine 37. (**B**) Amino acids involved in the three hydrogen bond networks at the Naa10–Naa15 interface: The first network (shown in orange) involves basic residues of Naa10 from the β4-α4 loop (Arg79 and Arg82) and amino acids from helix α23 and loop α24–α25 from Naa15 (Glu409, Asp438 and Asp441). The second network (shown in yellow) is constituted by acidic residues of the β2–β3 loop of Naa10 (Asp47 and Glu48) and amino acids of the α17 and α19 helices (Arg330 and Arg295) from Naa15. The third network (shown in pink) involves Glu24 and Asp140 from Naa10, two acidic residues located in the loops bordering the substrate-binding site, and Arg470 in the α26-α27 loop of Naa15. Ac-CoA is docked in the Naa10 subunit (sticks in CPK color). Note that the position of the side chain of Glu24 is highly mobile, yet it interacts with Arg470 via hydrogen bonds with occupancy of 0.9 during the simulation (Supplemental Material, Table S1). For the sake of overall clarity, we chose a snapshot where Glu24 does not interact with Arg470 (**C**). Amino acids that make hydrophobic contacts at the Naa10–Naa15 interface are shown as blue sticks. Interactions between Naa10 and Naa15 involve numerous hydrophobic contacts via helix α1 (Pro8, Met12, Leu19, Leu 20 and Pro23) and helix α2 (Met28, Phe32, Tyr33 and Leu36) of the Naa10 subunit and helices 25, 27, 28, 29 and 30 (Phe443, Met482, Trp486, Phe525, Tyr528 and Leu544) of the Naa15 subunit. (**D**) Superimposition of WT (cyan) and S37P (grey) Naa10. The S37P mutation shortens the α2 helix and modifies the protein flexibility in the two regions highlighted in orange (from N13 to E24 and E48 to E49).

free energy of binding, but are not affected by the S37P mutation (Supplementary Material, Fig. S3). The complex is also stabilized by three hydrogen-bonding networks represented in Figure 1B. Amino acids involved in the three hydrogen bond networks at the hNaa10–hNaa15 interface are shown as sticks in orange, yellow and pink, respectively. In both simulations, the mutation affects subtly but systematically two of these networks yielding a slight overall weakening of the interfacial hydrogen-bonding network (Supplementary Material, Table S1).

Comparison of the atomic fluctuations reveals differences in the flexibility of hNaa10-WT and S37P; the atomic fluctuations of helix α1 and loop α1–α2 decrease as a consequence of the S37P mutation of hNaa10 and this is observed in both MD replicates (Fig. 1D; Supplementary Material, Fig. S4).

Interestingly, this region lining the substrate-binding site is also involved in the hNaa10–hNaa15 interface. Amino acid Glu24 earlier identified as important for both catalytic activity and substrate binding (23) also mediates hydrogen bonding

with Arg470 of hNaa15 in the WT complex. In addition, in the mutant, we observe an increase of the flexibility of the β2–β3 loop, which carries Glu48, itself involved in hydrogen bonds with hNaa15. These alterations of the flexibility are also observed in independent 20 ns-long simulations of uncomplexed hNaa10-S37P. Moreover, we earlier reported correlations between the dynamics of the α2 helix and the peptide substrate-binding site of the structurally related hNaa50 (41).

Taken together, the predicted perturbations of the hNaa10–hNaa15 interactions and changes in the flexibility of key regions for substrate binding may result in impaired Nt-acetyltransferase activity and complex stability of human NatA-S37P.

hNaa10-S37P has impaired peptide substrate binding and reduced *in vitro* catalytic activity

In order to study if hNaa10-S37P displays a reduced catalytic activity, we assayed hNaa10-WT and hNaa10-S37P by a quantitative *in vitro* acetylation assay using three different Naa10 oligopeptide substrates represented by the N termini of classical *in vivo* human NatA substrates; SMCA4 (STPD-), the RNaseP protein p30 (AVFA-) (1) and γ-actin (EEEI-), the latter representative of a very efficient substrate *in vitro* and a likely posttranslational target of monomeric hNaa10 *in vivo* (28). The *in vitro* acetylation screen showed a 20–75% reduction in product formation for hNaa10-S37P dependent on the N-terminal sequence of the substrate oligopeptides tested (Fig. 2A). Further, the K_m, k_{cat} and specificity constants of the two enzymes were determined, both for the substrate oligopeptides and for Ac-CoA, to directly compare the catalytic efficiency of hNaa10-WT and hNaa10-S37P and their specificity for different substrates. The specificity constant k_{cat}/K_m of hNaa10-S37P was calculated to be 4-, 3.5- and 2-fold lower for the substrates EEEI, STPD and Ac-CoA, respectively, compared with hNaa10-WT (Fig. 2; Supplementary Material, Fig. S5). The mutant hNaa10 showed a ∼2-fold increase in K_m for the substrate oligopeptides EEEI and STPD, while no difference was observed for the K_m of Ac-CoA. Taken together, these data suggest that the S37P mutation reduces the intrinsic catalytic activity of hNaa10, likely due to altered peptide substrate binding or release, while Ac-CoA binding remains unaffected.

X-chromosome skewing supports the role of NAA10 in Ogden syndrome

Female mammals compensate dosage differences of X-chromosomal gene products by transcriptional silencing of one of the two X-chromosomes. This process, called X-chromosome inactivation (XCI), occurs during early development and is transmitted through subsequent mitosis (42). Although early studies suggest that the choice for which X-chromosome is inactivated is random (43), later studies on female carriers of specific X-linked mutations showed skewed patterns of XCI resulting from negative selection of cells harboring the lethal allele in the active state (44). Furthermore, X-chromosome skewing is a common feature of tumorigenic processes in which an acquired somatic mutation occurs in a single progenitor cell that subsequently undergoes clonal expansion and gives rise to progeny with the same XCI pattern (44, 45).

Therefore, we analyzed Ogden carrier women for their XCI pattern. First, a classical assay using the androgen receptor was used to determine the inactivation pattern in B cells from the Utah family (Fig. 3A). As shown in Figure 3B, the two female non-carriers show X-inactivation that is within the normal range, while all carriers have significant skewing. Three of the four carriers are nearly completely skewed; while the fourth (II-2) is less skewed (∼90%), although interpretation of this sample is complicated by alleles that are close in size (resulting in interference from stutter peaks). To assess the inactivated *NAA10* allele directly, a customized assay was performed. Supplementary Material, Figure S6B shows a representative result (for carrier woman II2). In all carrier women analyzed, the affected allele was found to be skewed toward the wild-type allele. These results support the hypothesis that cells expressing only the mutant *NAA10* allele might be counterselected for (at least B-cells) due to their decreased fitness or production rate.

Unaffected hNaa10 protein levels and subcellular localization in B cells and fibroblasts from Ogden males

To determine whether the hNaa10-S37P mutant had an impact on NatA subunit steady-state protein levels, protein profiles of EBV-immortalized B-cells were established and investigated for 11 members of the Ogden syndrome family including two males carrying the mutation and four female heterozygous carriers (Fig. 3A). Western blotting with specific NAT-antibodies demonstrated only minor mutation-correlated alterations in the steady-state protein levels of hNaa10 itself, the auxiliary subunit hNaa15 (21) or the physically associated hNaa50 (24) (Fig. 3C). These results and data from fibroblasts below suggest that the hNaa10-S37P mutation does not significantly alter protein levels of hNaa10 or other NatA components.

Primary fibroblasts isolated from one of the Ogden-affected males (III-6) and control BJ fibroblasts were immortalized in parallel by ectopically expressing the catalytic subunit of human telomerase (hTERT) (46,47). These are referred to as WT-hTERT for the BJ control cells and S37P-hTERT for the hNaa10-S37P-expressing cells (III-6 cells). A subcellular localization study of hNaa10 and hNaa15 by immunofluorescence demonstrated a similar and predominant cytoplasmic staining pattern for both WT and mutant protein and no obvious localization differences between WT- and S37P-hTERT were observed (Fig. 3D). Thus, neither the levels nor the subcellular localization of hNaa10 appear to be affected by the S37P mutation.

Ogden syndrome fibroblasts display altered proliferation, growth and migration

We further performed phenotypic analyses of the Naa10-S37P cells. S37P-hTERT cells displayed a significantly increased cell size compared with the control cell line (Fig. 4A). In dense cultures, it was also evident that S37P-hTERT cells packed differently compared with control cells and started to grow on top of each other (Fig. 4B). In analogy to cancer cell lines, these findings suggest a partial loss of cell-to-cell contact inhibition when they reach confluence. These data are supported by cell cycle analyses (fluorescence-activated cell sorting, FACS) that show that at least 9% of S37P-hTERT cells continue to proliferate when in dense culture, while WT-hTERT cells enter the G0 phase (Supplementary Material, Fig. S7). The migration capacity was assessed by a wound-healing assay where cells were inspected every 15 min for a total of 48 h (Fig. 4C; Supplementary Material, Fig. S8). S37P-hTERT cells were impaired in their motility both in normal growth medium and particularly when culturing cells in poor medium (medium lacking either serum or L-glutamine). Importantly, when overexpressing hNaa10-WT in S37P-hTERT cells, a partially rescued migration potential was observed. Furthermore, cell proliferation assays with cells seeded at different densities all showed a significantly reduced growth rate for S37P-hTERT cells

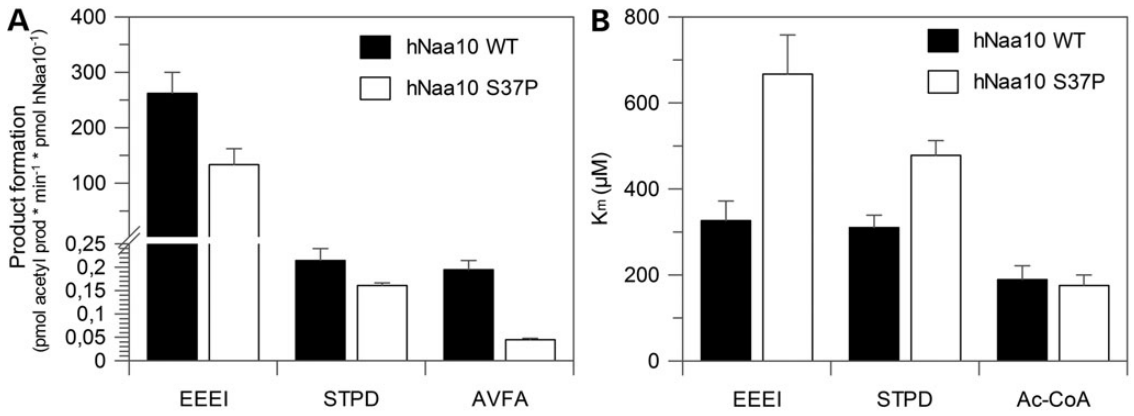

C

	EEEI		STPD		Ac-CoA	
	WT	S37P	WT	S37P	WT	S37P
Km (µM)	326,5 ± 46,4	667,0 ± 91,5	310,9 ± 28,9	478,3 ± 34,7	189,2 ± 31,8	175,6 ± 24,1
kcat/Km (M^{-1}* s^{-1})	$13,1*10^3$ ± $2,0*10^3$	$3,2*10^3$ ± $0,5*10^3$	6,3 ± 0,5	1,8 ± 0,2	$28,6*10^3$ ± $5,3*10^3$	$15,4*10^3$ ± $2,2*10^3$

Figure 2. *In vitro* NAT-activity and kinetic parameters of hNaa10-WT and hNaa10-S37P. (**A**) NAT activity of the recombinant MBP-hNaa10-WT and MBP-hNaa10-S37P for oligopeptides EEEI, STPD and AVFA. Purified MBP-hNaa10-WT/S37P was incubated with 2 mM peptide and 500 µM Ac-CoA for 10 min, and the reaction was stopped by adding TFA to a final concentration of 1%. Product formation was quantified by RP-HPLC, $P < 0.001$ (**B**) Apparent K_m values of MBP-hNaa10-WT/S37P for the synthetic oligopeptides EEEI ($P < 0.01$), STPD ($P < 0.01$) and for Ac-CoA. Purified MBP-hNaa10-WT/S37P was incubated with varying concentrations of either peptide or Ac-CoA in acetylation buffer for 10 min at 37°C. The K_m and k_{cat} were determined with the software GraFit7 (**C**) Summary of the K_m and k_{cat}/K_m values of MBP-hNaa10-WT/S37P for oligopeptides EEEI, STPD and for Ac-CoA.

when compared with WT-hTERT cells (Fig. 4D). Notably, decreased growth rate and proliferation of Ogden cells were also confirmed for primary WT and Ogden S37P fibroblasts (III-6; Supplementary Material, Fig. S9). A WST-8 viability assay (Fig. 4E) demonstrated that the S37P-hTERT cells were less viable when cultured dispersed (1000 cells per well in a 96-well tray). However, the WST-8 assay also revealed that the S37P-hTERT cells were metabolically more active when kept in a dense culture. Selected markers for pathways linked to Naa10's function revealed that Ogden syndrome fibroblasts have higher levels of Retinoblastoma 1 (Rb1), a known negative regulator of the cell cycle (Fig. 4F) (48–50). Myosin light chain kinase (MYLK), and thereby cell motility, was previously shown to be positively regulated by hNaa10 by a direct interaction (51). Here, we were not able to demonstrate an interaction between hNaa10 and MYLK in either WT- or S37P-hTERT cells (Supplementary Material, Fig. S10). Rb1 was previously found to be affected in specific thyroid cancer cells upon hNAA10 depletion (52). Other pathways, including cyclin D1/β-catenin, TSC2/mTOR/pS6K1 and β-PIX (ARHGEF7) (53–55) did not appear to be perturbed in S37P-hTERT cells (Fig. 4F; Supplementary Material, Fig. S10). Summarizing this part, Ogden syndrome fibroblasts display an altered morphology, growth and migration pattern and are more sensitive towards stressed conditions, a phenotype that was partially rescued upon overexpressing hNaa10-WT in S37P-hTERT cells (Fig. 4C).

hNaa10-S37P impairs NatA complex formation and intrinsic NatA catalytic activity

The structural modeling and MD simulations suggested that NatA (hNaa10–hNaa15) complex formation could be negatively affected by the hNaa10-S37P mutant. This was investigated by co-expression of hNaa15-myc and hNaa10-V5 or hNaa10-S37P-V5 followed by co-immunoprecipitation from HEK293 cells. It was evident that NatA complex formation was impaired when expressing hNaa10-S37P-V5 when compared with hNaa10-V5 (Fig. 5A). This finding was confirmed in co-immunoprecipitation studies detecting endogenous proteins (Fig. 5B, left panel). We also showed that complex formation of hNaa10 with hNaa50 was reduced in the context of NatA-S37P mutant (Fig. 5B, right panel). In order to study complex formation of endogenous NatA and NatA-S37P complexes, lysates of WT- and S37P-hTERT cells were subjected to immunoprecipitation using anti-hNaa10 or anti-hNaa15. The NatA complex was detectable in both cell types, but the ability of hNaa10-S37P to interact with hNaa15 was significantly reduced (Fig. 5C). As the *in vitro* kinetic studies suggested that hNaa10-S37P is catalytically impaired, we also assessed the *in vitro* NAT activity of the endogenous hNaa10 in complex with hNaa15. NatA complexes were immunoprecipitated from WT- and S37P-hTERT cell lysates, and the absolute catalytic activity of NatA-S37P was measured. As expected, NatA-S37P activity towards the SESS-starting substrate oligopeptide was significantly reduced when compared with NatA-WT when correlating the amount of hNaa15 present in each sample (NAT activity per hNaa15 molecule; Fig. 5D, left). When correlating the amount of hNaa10 (NAT activity per hNaa10 molecule; Fig. 5D, right) an ~10-fold reduction was measured. Combined, these results suggest that hNaa10-S37P is partially defective in both its ability to bind hNaa15 and in its catalytic activity.

Reduced protein N-terminal acetylation levels in B cells and fibroblasts derived from males with Ogden syndrome

N-Terminal-combined fractional diagonal chromatography (COFRADIC) has previously been used to quantify the degree

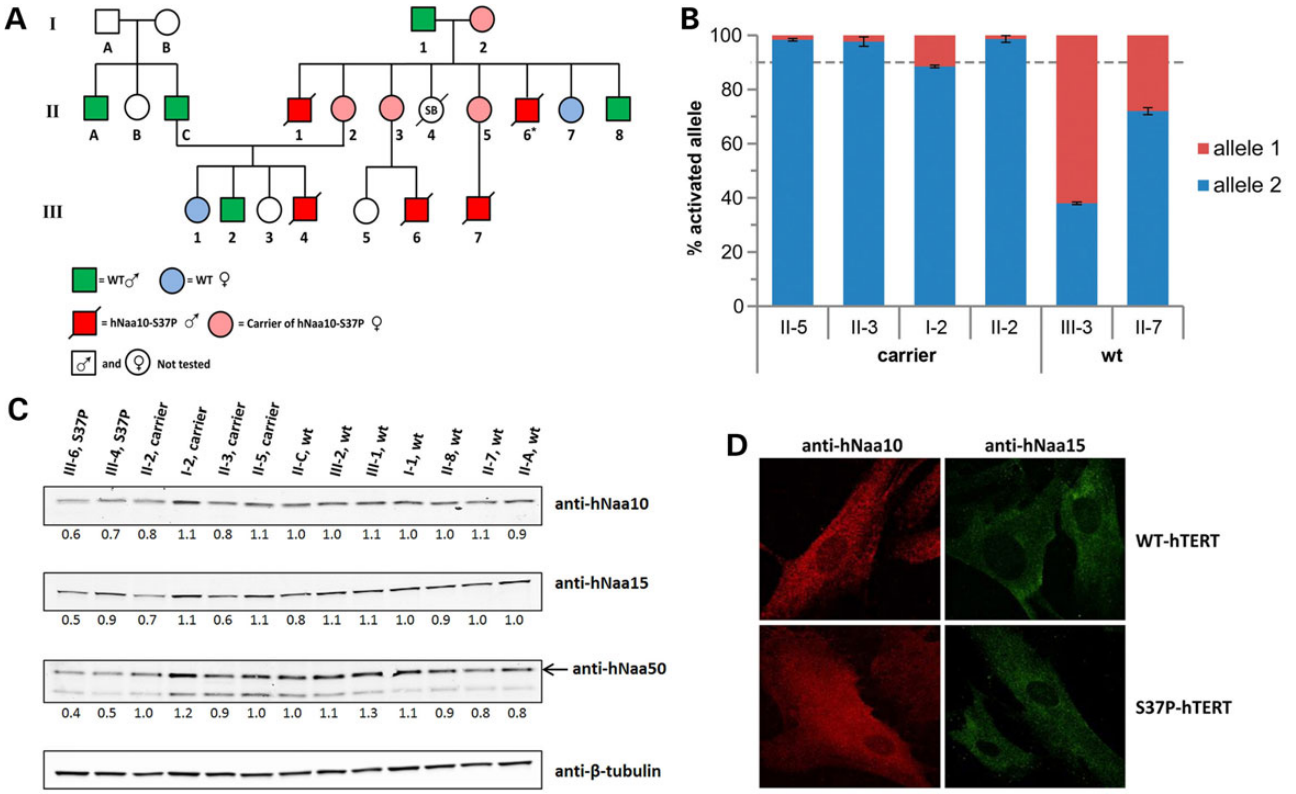

Figure 3. X-chromosome skewing among female carriers and hNaa10-S37P protein parameters in patient-derived cells. (**A**) The pedigree of the Ogden syndrome family. hNaa10-WT family members indicated with green squares for male individuals and blue circle for female individuals. Infant males with S37P indicated with a red square and healthy women carriers of the S37P mutation indicated with a pink circle. *, presumed to have the mutation. (**B**) X-chromosome inactivation assay. Classical X-chromosome inactivation analysis using exon 1 of human androgen receptor locus. Shown is the quantitative evaluation of the XCI pattern for six members of the Utah family. An inactivation pattern of >90% is considered to be skewed. All females from the Ogden syndrome family have been tested for X-inactivation at least twice. (**C**) Immortalized B cells from family members were lysed and analyzed by SDS–PAGE and western blotting using anti-hNaa10, anti-hNaa15 or anti-hNaa50 antibodies. Anti-β-tubulin was used as control for equal protein loading. The levels of hNaa10, hNaa15 and hNaa50 were quantitated by densitometry analysis (ImageJ) where each band of hNaa10/hNaa15/hNaa50 was corrected to its corresponding β-tubulin level and further normalized to the other samples where the mean value of all WT samples was set to 1.0. (**D**) Confocal micrographs (×67 magnification) of hTERT-transduced fibroblasts; WT-hTERT (BJ-hTERT), S37P-hTERT stained with anti-hNaa10 (red) or anti-hNaa15 (green) and counter-stained with Alexa Fluor 594 or Alexa Fluor 488 secondary antibody. Images shown are representative of at least 50 observed cells.

and define the patterns of *in vivo* protein Nt-acetylation (1,5,56) and was here used to investigate whether patient cells derived from affected males or female carriers displayed altered levels of protein Nt-acetylation at the proteome-wide level. By *in vitro* labeling with $^{13}C_2D_3$-acetylation, all Nt-free amines are modified with an $^{13}C_2D_3$ acetate moiety, allowing us to distinguish between *in vivo* Nt-acetylated and primary protein N termini and to quantify the degree of Nt-acetylation (57). Overall, 2624 human N termini derived from 2346 human proteins were identified in all B-cell samples analyzed (Supplementary Material, Tables S2 and S3). Of these 2624 N termini, 2067 started at Position 1 or 2 (1970 proteins), while 557 had a start position beyond protein Position 2 (510 proteins). The latter N termini are indicative of alternative translation initiation events (58,59). Four hundred and seventy-two of all N termini were identified in all setups analyzed (18% of all identified protein N termini).

Comparing the Nt-acetylomes of Ogden syndrome male III-4 and his brother III-2 (hNaa10-WT) allowed us to identify differences in the degree of Nt-acetylation of 1066 N termini. Here, the hNaa10-S37P mutation resulted in a reduced degree of *in vivo* Nt-acetylation of a subset of N termini; 30 N termini (3% of all N termini) displayed a difference of 10% or more in their degree of Nt-acetylation (Supplementary Material, Tables S2–S5), while the degree of Nt-acetylation remained essentially unaltered when comparing Nt-acetylomes of carriers and WT samples (see Supplementary Material, Fig. S11 for a correlation of all family members with a healthy hNaa10-WT brother (III-2) of an Ogden syndrome male).

Representative MS-spectra of a classical NatA-type substrate, an Ala-starting N-terminal peptide from the translational activator GCN1 (A_2ADTQVSETLKR$_{13}$) (Fig. 6A) and of a possible NatE substrate, the Met-Leu-starting N-terminal peptide of the Kinesin-like protein (M_1LGAPDESSVR$_{11}$) (Fig. 6B), are shown for an Ogden syndrome male (III-4, hNaa10-S37P) and his brother (III-2, hNaa10-WT) and a reduced degree of Nt-acetylation is in both cases clearly visible (Supplementary Material, Fig. S11 and Tables S2–S4; Table 1). These peptides were found to be Nt-acetylated between 50 and 54% in the proteomes of B cells derived from two males with Ogden syndrome in comparison with 77–86% in the proteomes of unaffected individuals, thus showing a reduced degree of Nt-acetylation of 28 and 25% on average, respectively (Supplementary Material, Table S2). Figure 6C shows representative scatter plots displaying the correlation of the degrees of Nt-acetylation of all determined and commonly identified N termini in the N-terminal proteomes of an Ogden syndrome male (III-4, hNaa10-S37P) and his brother (III-2, hNaa10-WT) (left panel), and the brother (III-2, hNaa10-WT) and his mother (II-2, carrier of hNaa10-S37P) (right panel).

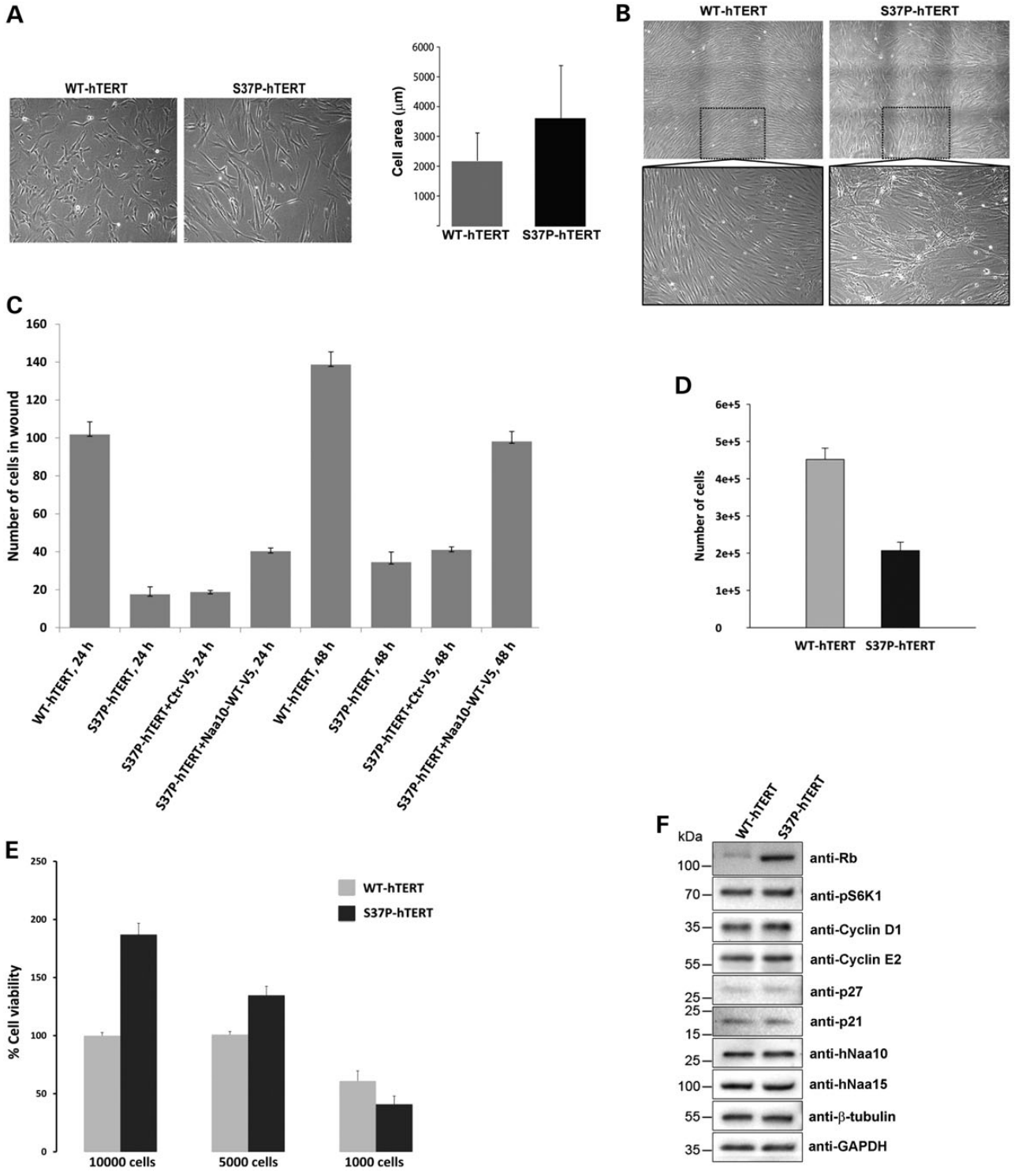

Figure 4. Altered size, morphology, growth rate and migration capacity of S37P-hTERT fibroblasts cells. (**A**) Live imaging (10×) of WT-hTERT (hNaa10-WT) and S37P-hTERT (hNaa10-S37P) cells with cell size measurements of 100 cells of each type. The cell size is indicated in micrometer squared and the difference between WT- and S37P-hTERT was statistically significant ($P < 0.001$, Student's *t*-test). (**B**) Live imaging (10×) of dense WT- and S37P-hTERT cultures demonstrating cell packing. Upper panel: nine overlapping live cell images of WT- or S37P-hTERT; lower panel: zoom-in on delineated field. (**C**) Wound-healing experiment where cell migration of WT- and S37P-hTERT was monitored every 15 min for 48 h. S37P-hTERT cells were transfected with pcDNA3.1-V5 vector (S37P-hTERT+Ctr-V5) or pcDNA3.1-Naa10-WT-V5 (S37P-hTERT+Naa10 WT-V5). Total number of cells migrating in the wound as indicated showed a statistically significant difference between WT- and S37P-hTERT cells ($P < 0.0001$, Student's *t*-test) as well as between S37P-hTERT+Ctr-V5 and Naa10-S37P+Naa10 WT-V5 cells ($P < 0.0001$, Student's *t*-test). (**D**) Proliferation assay with cells seeded at Day 1 and counted 1 week later. (**E**) WT- and S37P-hTERT cells were seeded dispersed (1000 cells) and dense (5000 and 10 000 cells) per well in a 96-well tray and incubated for 16 h, before being subjected to cell viability/metabolic activity assay (WST-8). (**F**) WT- and S37P-hTERT protein lysates analyzed by western blotting using anti-Rb, anti-pS6K1, anti-cyclin D1, anti-cyclin E2, anti-p27, anti-p21, anti-hNaa10 and anti-hNaa15. β-Tubulin and GAPDH were used as a control for equal protein loading.

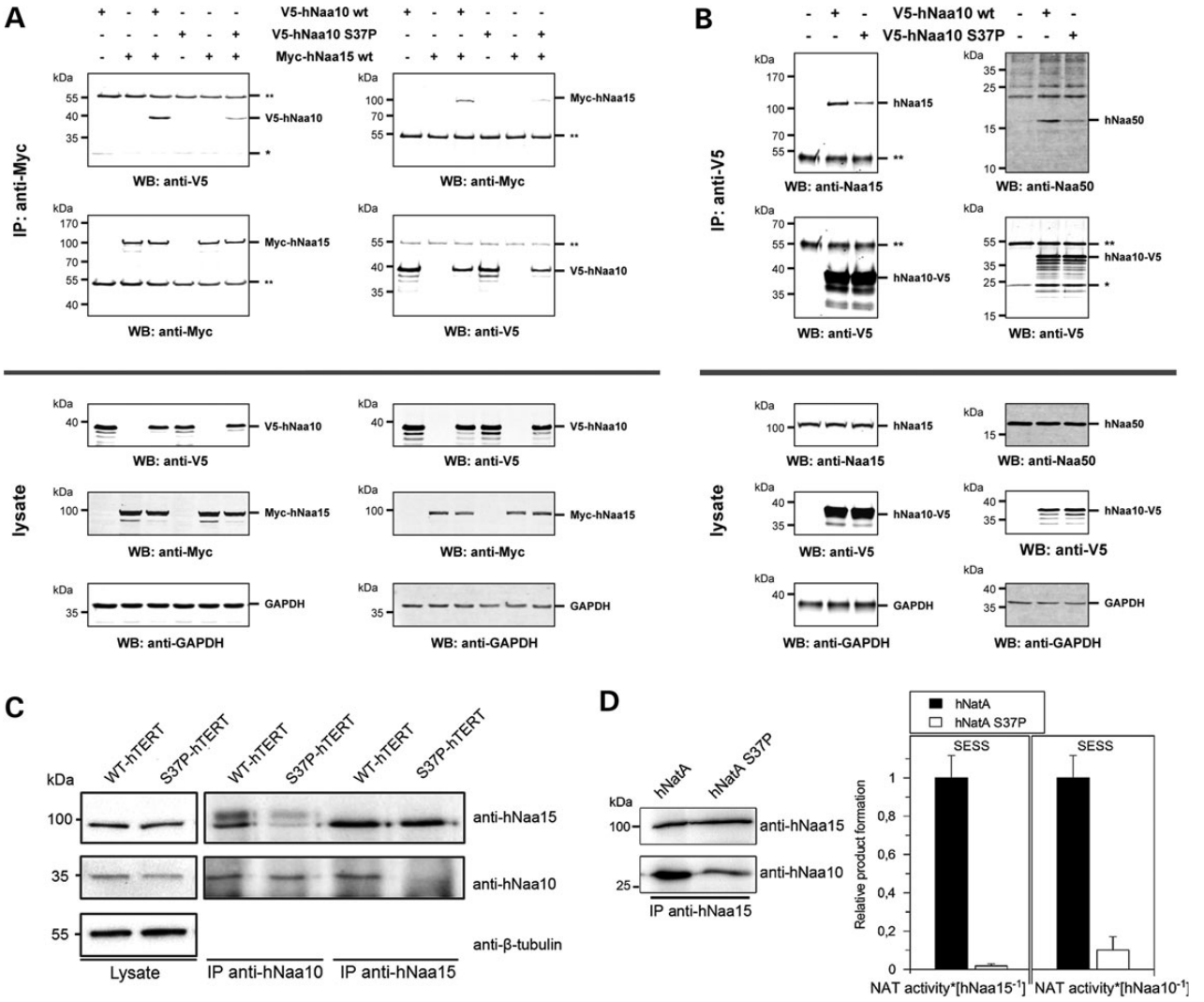

Figure 5. Reduced human NatA complex formation and catalytic activity of hNaa10-S37P. (**A**) HEK293 cells were transiently transfected with hNaa10-V5 and hNaa15-Myc encoding plasmids and hNaa10-V5 or hNaa15-Myc was immunoprecipitated using anti-V5 or anti-Myc antibodies, respectively (upper panel). Loading and transfection controls are shown in the lower panel. ** and *, respectively, indicate heavy and light chain of precipitating antibody. GAPDH levels indicate equal input. (**B**) Co-immunoprecipitation of transfected HEK293 cells with endogenous Naa15 (left) or Naa50 (right). ** heavy and * light chain of precipitating antibody. (**C**) Endogenous hNatA was immunoprecipitated from WT- and S37P-hTERT fibroblasts using either anti-hNaa10 or anti-hNaa15 and analyzed by western blotting using anti-hNaa15 or anti-hNaa10. β-Tubulin levels indicate equal input. Lysates (Lanes 1 and 2) show equal amount of the hNaa10 and hNaa15 proteins at the start. (**D**) hNatA and hNatA-S37P was immunoprecipitated from WT- and S37P-hTERT cell lines, respectively, with anti-hNaa15 and used for NAT-activity measurements towards the substrate polypeptide SESS. The amount of hNaa10 and hNaa15 present in each sample was determined by western blotting and densitometry analysis by the use of ImageLab v3.0. Activity measurements were correlated to band intensities to show relative product formation (activity) per hNaa10 or hNaa15 molecule present in each sample. hNatA activity was set to 1 and hNatA S37P activity was calculated relative to this. All data shown are representative of three independent experiments.

Further, all affected N-termini display a reduced degree of Nt-acetylation in the proteomes of B cells derived from males with Ogden syndrome when compared with unaffected individuals. Overall, N-terminomics demonstrated reduced N-terminal acetylation of classical NatA-type substrates, as well as some NatE-type substrates for Ogden syndrome affected individuals.

Differential N-terminal COFRADIC analyses were also performed to check the protein Nt-acetylation states in fibroblasts carrying the S37P mutation. WT, WT-hTERT, S37P and S37P-hTERT fibroblasts were stable-isotope labeling by amino acids in cell culture (SILAC) labeled and their N-terminomes were compared, assaying the corresponding wild-type and mutant cell lines alongside. The distribution of N-terminal peptides based on their Nt-acetylation status and their known/predicted Nat-substrate class in the proteomes of these fibroblasts is shown in Figure 7A. The overall degree of Nt-acetylation (82%) and the Nat-type distribution of identified protein N termini in the fibroblast proteomes showed a clear resemblance to the B-cell proteomes (Supplementary Material, Table S2) as well as to earlier studies in human cancer cells (1,5). About 57% of the N-terminome consists of typical NatA-type peptides, 20% NatB substrates, 5% NatC/NatE or NatF substrates, while 18% was Nt-free (Fig. 7A). The latter group included peptides with Pro at Position 1 or 2, known as Nt-free N termini (3), and additionally hold N termini from other Nat-type classes with <2% Nt-acetylation *in vivo*. As for the B cells, N-terminal proteomics revealed a reduced N-terminal acetylation of classical/predicted NatA-type substrates, both in primary and hTERT-immortalized S37P fibroblasts (Fig. 7A–E and Table 1; Supplementary Material, Tables S6 and S7). Representative MS-spectra of N-termini displaying

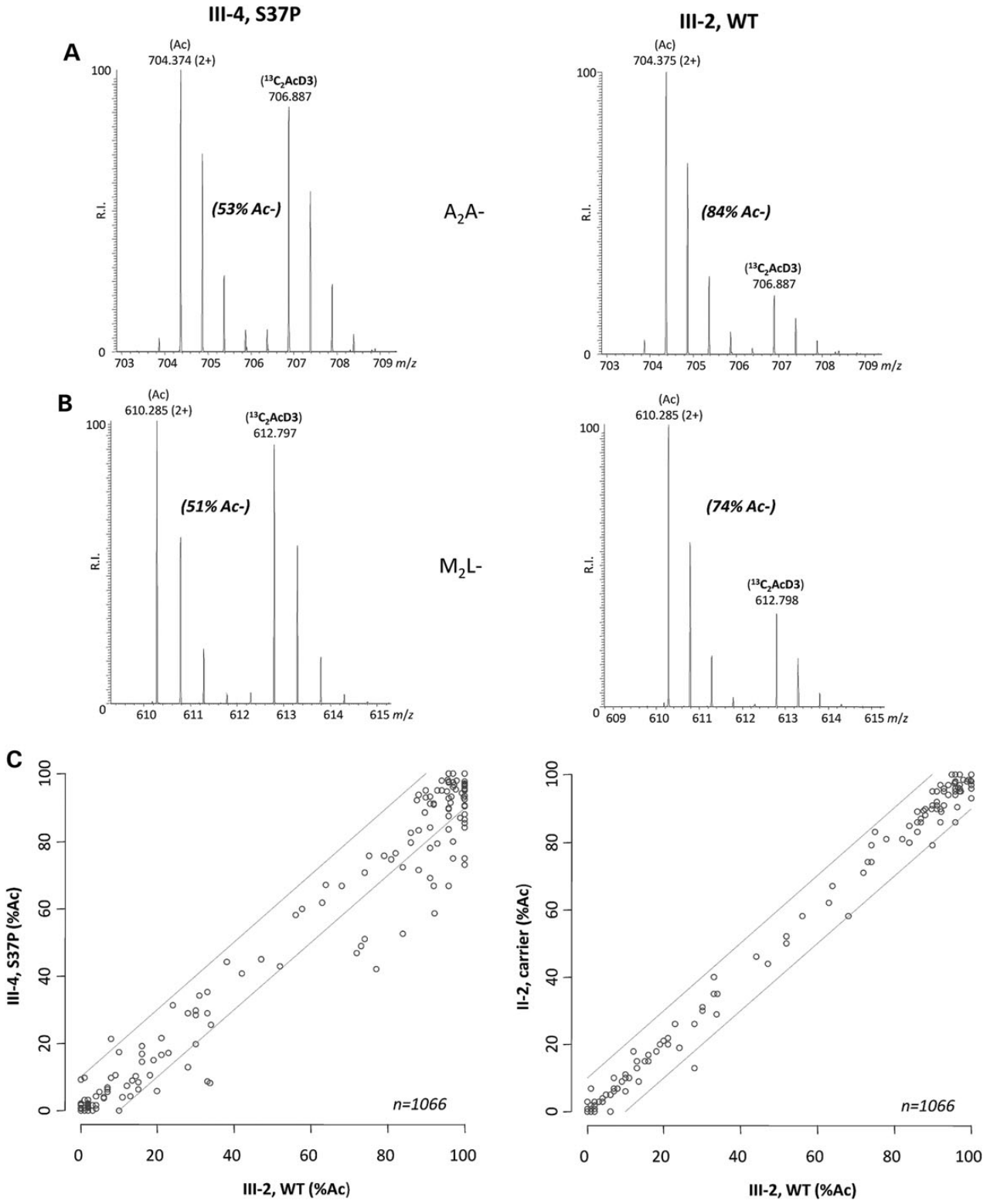

Figure 6. Impaired *in vivo* Nt-acetylation in B cells from Ogden syndrome patients. N-Terminal- COFRADIC was used to enrich protein N termini and quantify their degree of *in vivo* protein Nt-acetylation. (**A**) Representative MS-spectra of an Ala-starting N-terminal peptide (classical NatA-type substrate), here the translational activator GCN1 (A_2ADTQVSETLKR$_{13}$) and (**B**) the ML-starting N-terminal peptides (NatE substrate), of the Kinesin-like protein (M_1LGAPDESSVR$_{11}$) are shown for an Ogden syndrome male (III-4, hNaa10-S37P), left panel and his brother (III-2, hNaa10-WT), right panel, respectively. (**C**) Representative scatter plots displaying the correlation of the degrees of Nt-acetylation of all N termini identified in the N-terminal proteomes of patient III-3 (brother, hNaa10-WT) and III-4 (proband, hNaa10-S37P), left panel and patient III-2 (brother, hNaa10-WT) and II-2 (mother, carrier of hNaa10-S37P), right panel.

Table 1. Overview of N termini less acetylated in Naa10-S37P B-cells, fibroblasts and siNatA HeLa cells

NAT type	P1′[a]	P1–P5[b]	S37P B-cells	S37P fibroblasts	siNatA (HeLa)	Accession	Protein description
NatA	M	AAADA	√	NI	NI	Q9H9B1	Histone-lysine N-methyltransferase EHMT1 (EHMT1)
NatA	M	AAAEE	√	√	NI	Q99942	E3 ubiquitin-protein ligase RNF5 (RNF5)
NatA	M	AAAQE	√	√	NI	O96005	Cleft lip and palate transmembrane protein 1 (CLPT1)
NatA	M	AADTQ	√	√	√	Q92616	Translational activator GCN1 (GCN1L)
NatA	M	AAESA	√	√	√	Q14241	Transcription elongation factor B polypeptide 3 (ELOA1)
NatA	M	AAGGG	√	√	NI	Q5VT52	Regulation of nuclear pre-mRNA domain-containing protein 2 (RPRD2)
NatA	M	AEVQV	√	√	√	P40429	60S RL13A
NatA	M	AGGGA	NI	√	NI	Q13637	Ras-related protein Rab-32 (RAB32)
NatA	M	AGPLQ	√	√	NI	Q9P015	39S ribosomal protein L15, mitochondrial (RM15/MRPL15)
NatA	M	AIKSI	NI	√	NI	Q9Y2C4	Nuclease EXOG, mitochondrial (EXOG)
NatA	M	ALDGP	√	√	NI	P62195	26S protease regulatory subunit 8 (PRS8)
NatA	M	AQPGT	√	NI	NI	Q8NEF9	Serum response factor-binding protein 1 (SRFB1)
NatA	M	ASAGS	NI	√	NI	Q9BQJ4	Transmembrane protein 47 (TMM47)
NatA	M	AVEDE	√	√	NI	Q14644	Ras GTPase-activating protein 3 (RASA3)
NatA	M	AVFAD	√	√	√	P78346	Ribonuclease P protein subunit p30 (RPP30)
NatA	M	AVKVQ	NI	√	NI	O75746	Calcium-binding mitochondrial carrier protein Aralar1 (CMC1)
NatA	M	GAAAA	NI	√	NI	Q9Y580	RNA-binding protein 7 (RBM7)
NatA	M	GAVTD	√	√	NI	Q6I9Y2	THO complex subunit 7 homolog (THOC7)
NatA	M	GEQPI	√	NI	NI	Q86YM7	Homer protein homolog 1 (HOME1)
NatA	M	SASVV	√	√	NI	P61803	Dolichyl-diphosphooligosaccharide-protein glycosyltransferase subunit DAD1 (DAD1)
NatA	M	SEGDS	NI	√	NI	O15258	Protein RER1 (RER1)
NatA	M	SGFLE	√	√	NI	O95807	Transmembrane protein 50A (TM50A)
NatA	M	TAQGG	√	√	NI	Q5J8M3	Transmembrane protein 85 (TMM85)
NatA	M	TKAGS	√	√	NI	Q96AG4	Leucine-rich repeat-containing protein 59 (LRC59)
NatA	M	TKVAE	√	NI	NI	Q13206	Probable ATP-dependent RNA helicase DDX10 (DDX10)
NatA	M	TMDAL	√	NI	NI	Q86XL3	Ankyrin repeat and LEM domain-containing protein 2 (ANKL2)
NatA	M	TMDKS	√	√	NI	P31946	14-3-3 protein β/α (1433B)
NatA	M	VEKEE	√	√	√	Q9UBE0	SAE1
NatA	M	VEQGD	√	NI	NI	A4D1U4	Protein LCHN (LCHN)
NatA	M	VEYVL	√	NI	NI	Q8TB72	Pumilio homolog 2 (PUM2)
NatA	M	VNPTV	√	√	√	P62937	Peptidyl-prolyl *cis–trans* isomerase A (PPIA)
NatA	M	VTMEE	√	NI	NI	Q13115	Dual specificity protein phosphatase 4 (DUS4)
NatE[c]	–	MLEAM	√	NI	NI	Q9BUL5	PHD finger protein 23 (PHF23)
NatE[c]	–	MLGAP	√	NI	NA	Q7Z4S6	Kinesin-like protein KIF21A (KI21A)
NatE[c]	–	MLSPE	√	NI	NI	Q9NUG6	p53 and DNA damage-regulated protein 1 (PDRG1)
NatE[c]	–	MMDPC	√	NI	NI	Q8N8R7	Uncharacterized protein C11orf46 (CK046)
NatE[c]	–	MVEKE	√	√	NA	Q9UBE0	SAE1
NatE[c]	–	MVNPT	√	√	NI	P62937	Peptidyl-prolyl *cis–trans* isomerase A (PPIA)
NatE[c]	–	MVTEQ	√	√	NI	Q9BU89	Deoxyhypusine hydroxylase (DOHH)

[a]iMet cleaved off prior to Nt-acetylation.
[b]First five amino acids of the acetylated peptide.
[c]Putative NatE substrate.
NI, respective N termini were not identified; NA: respective N termini were identified, but not affected under the conditions assayed.

an ~30 or ~40% difference in their Nt-acetylation status in S37P cells when compared with control WT primary cells as well as hTERT cells are shown for the Ser-starting dolichyl-diphosphooligosaccharide-protein glycosyltransferase subunit (DAD1) and the Ala-starting mitochondrial ribosomal protein L15 (MRPL15) (Fig. 7B–E). No major differences in Nt-acetylation levels were observed between primary and hTERT-immortalized cells (Supplementary Material, Table S6).

Overall, in B cells as well as in fibroblasts, a fraction of the N-terminal acetylome was affected by the hNaa10-S37P mutation, and the affected N termini mostly represented classical NatA substrates and some putative NatE substrates (Figs 6 and 7 and Table 1; Supplementary Material, Table S4), the latter consistent with the reduced hNaa10 interaction demonstrated above with hNaa50 (Fig. 5).

Characterization of hNaa10-S37P-affected Nt-acetylation substrates, including THOC7

In order to determine whether the substrates affected in their Nt-acetylation status in hNaa10-S37P cells depended on their Nt-acetylation for protein stability, we selected seven substrates for in-depth investigation: THO complex subunit seven homolog (THOC7), SUMO-activating enzyme subunit 1 (SAE1), transcription elongation factor B polypeptide 3 (ELOA1), 60S ribosomal protein L13a (RL13A), OTU domain-containing protein 7B (OTU7B),

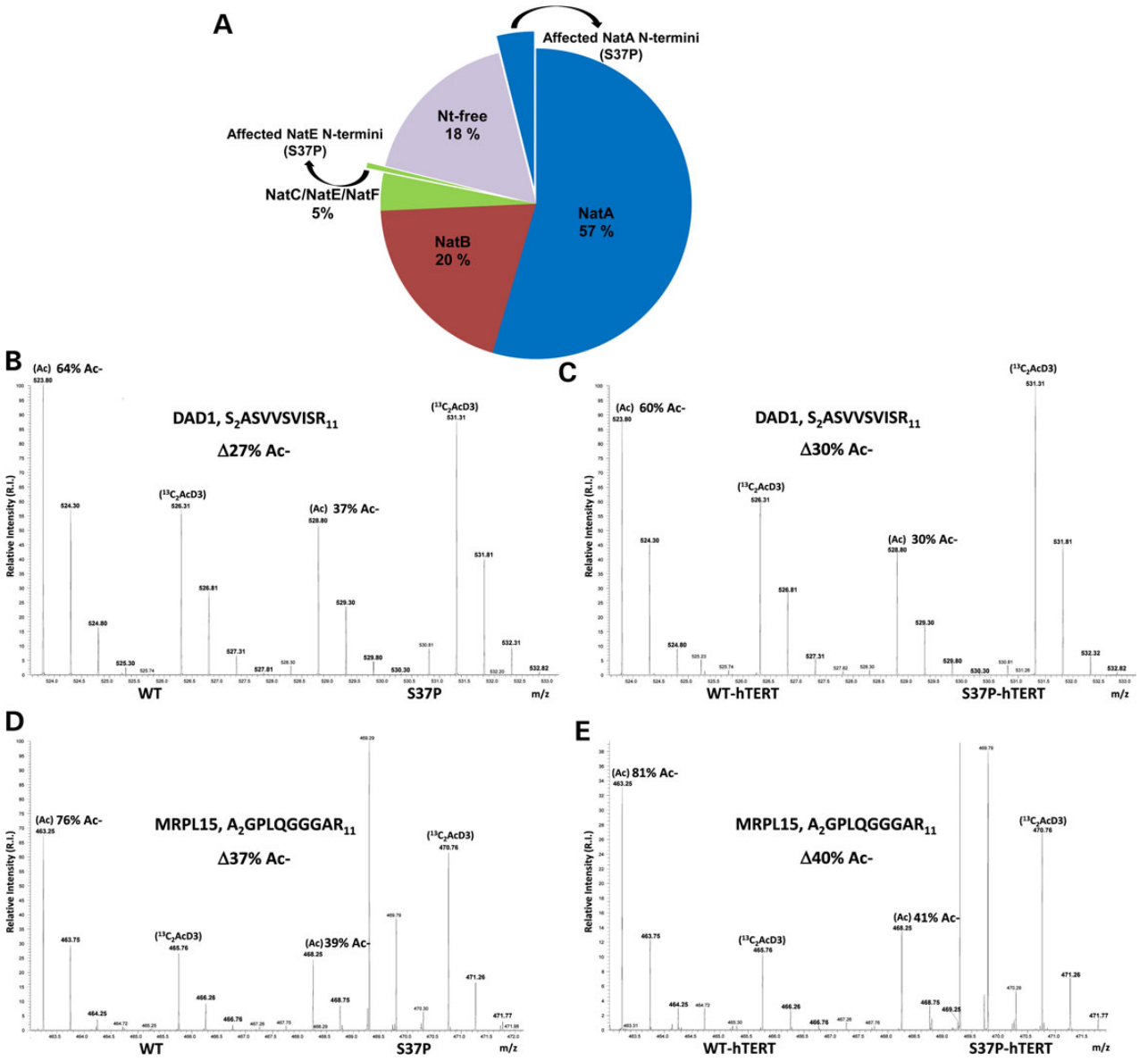

Figure 7. Effect of the hNaa10-S37P mutation in fibroblasts on specific subgroups of the Nt-acetylome and on the Nt-acetylation of individual proteins. (**A**) The distribution of N-terminal sequences according to Nt-acetylation status and NAT-type groups in the proteome of WT cells. The highlighted pie parts represent peptides with a ≥10% Nt-acetylation shift in S37P cells when compared with WT. (**B**) A representative MS spectrum of the N terminus of dolichyl-diphosphooligosaccharide-protein glycosyltransferase subunit (DAD1) in primary fibroblast WT cells and primary fibroblast S37P cells, while (**C**) shows the DAD1 MS spectrum in WT- and S37P-hTERT fibroblasts. (**D**) A representative MS spectrum of the 39S ribosomal protein L15 (MRPL15) in WT and S37P fibroblasts and (**E**) shows a typical MS spectrum of RM15 in WT- and S37P-hTERT fibroblasts.

DAD1 and MRPL15. It is well known that mutating the second residue in a protein to proline inhibits Nt-acetylation by the NATs (28,60). Therefore, these candidates and their Pro mutant versions were expressed and investigated by western blotting to probe their steady-state protein levels. None of the mutant (non-acetylated) proteins displayed a significant difference when compared with their wild-type variants except for THOC7 that showed significantly lower levels when expressed as an Nt-free, proline mutant. To verify these findings, the cDNAs of THOC7 (Fig. 8A) and SAE1 (Fig. 8B) were modified as follows; the codons for the second residue, respectively, encoding Gly (for THOC7) or Val (for SAE1) were replaced by an Ser, Pro, Val or Asp to promote full NatA- (4) (Ser-) or full NatB- (Asp-) dependent Nt-acetylation of the amino-terminus, to prevent Nt-acetylation (61) (Pro-) or to promote partial Nt-acetylation of the amino-terminus (6) (Val-). Furthermore, their degree of Nt-acetylation was determined using in-gel stable-isotope labeling (ISIL) followed by in gel-digestion and mass spectrometric analysis (62). In line with what was expected, the N termini of THOC7-WT (96%), THOC7-G2V (21%) and SAE1-WT (19%) were found to be partially Nt-acetylated, while THOC7-G2S, THOC7-G2D and SAE1-V2S were fully Nt-acetylated and the G2P variants were Nt-free (Fig. 8). Of note here is that only SAE1 variants with their iMet removed were detected in the setups analyzed. Overall, no notable differences in the steady-state, synthesis and degradation levels could be observed for the N-terminal SAE1 variants, while the THOC7-G2P and G2V variants displayed a decreased protein stability which was rescued upon proteasomal inhibition (Fig. 8A).

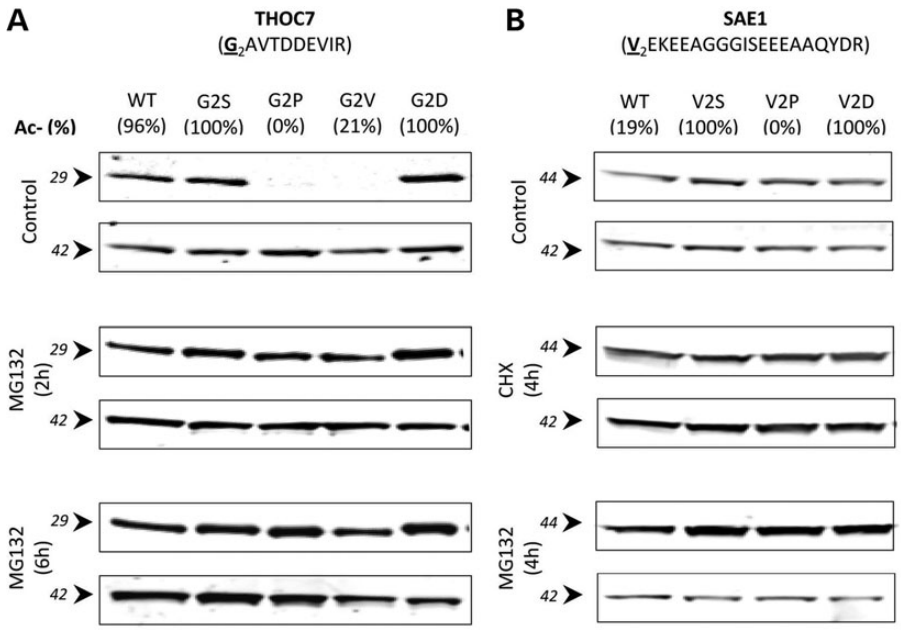

Figure 8. Steady-state expression levels of N-terminal variants of proteins identified as less Nt-acetylated in Naa10-S37P B-cells and fibroblasts. The cDNA of the WT THO complex subunit seven homolog (THOC7) (**A**) and the SAE1 (**B**) were subcloned into a C-terminal V5/His-tag pEF-DEST51 vector and a series of N-terminal mutants were created where the second amino acid was replaced by Ser, Pro, Val or Asp and transfected into A431 cells. After 24 h of expression, samples were taken of cells treated with either proteasomal inhibitor MG132 or the translation inhibitor cycloheximide (CHX). The tagged proteins were detected by western blotting using anti-V5 antibody and the degree of Nt-acetylation was assayed by ISIL.

To further unravel if Nt-acetylation of THOC7 affects the protein's half-life, THOC7-V5/His variants were expressed in untreated and siNatA-treated A431 cells and a cycloheximide chase was performed. THOC7 variants were immunoprecipitated using anti-V5 antibody and their degree of Nt-acetylation determined (Fig. 9A and B) (30,62). When silencing NatA (siNatA), the difference in protein half-life ($t_{1/2}$) increased by over 1.5-fold when comparing the THOC7-G2S and THOC7-WT chases. THOC7-G2S was fully Nt-acetylated in both setups while THOC7-WT Nt-acetylation drops from 96 to only 50% upon siNatA treatment. In fact, THOC7-WT showed a decrease in $t_{1/2}$ in the siNatA setup and approached the $t_{1/2}$ of free THOC7-G2P, indicating that a reduced degree of Nt-acetylation of THOC7, and not the N-terminal mutation introduced, is linked to the decrease in THOC7 protein half-life (Fig. 9A). Quantification of the CHX pulse-chase data revealed a decreasing protein stability for THOC7-G2D > G2S > WT > G2P > G2V (Fig. 9B). Figure 9C shows the sihNaa10 and sihNaa15 (siNatA) knockdown efficiency in A431 cells and revealed an NatA knockdown efficiency of ≥95%. Representative MS and MS/MS spectra for the Nt-acetylated status of THOC7-WT in siCtrl versus siNatA-treated knockdown A431 cells are shown in Figure 9D.

Discussion

Ogden syndrome is a genetic disorder with a wide variety of severe phenotypes and ultimately leads to mortality during infancy in males. The syndrome is associated thus far in two families with a single point mutation in hNAA10 creating an S37P substitution in the resulting protein. X-chromosome skewing analyses in the carrier women demonstrates skewing, consistent with either a production or an elimination defect for lymphocytes expressing the X-chromosome with the mutation in hNAA10. Consistent with this result, cell proliferation assays showed that both primary and TERT-immortalized hemizygous S37P-hTERT cells derived from one of the male infants have a reduced growth rate compared with standard control cells. One caveat is that these cell lines were non-isogenic, and as such genetic background differences could contribute to the different growth rates observed between these two fibroblast cell lines. However, the altered growth rate is in agreement with several studies in cancer cells demonstrating that loss of NatA or hNaa10 affects cell proliferation via several different pathways (35). One of these pathways, the Rb1-pathway, was also found to be affected in the S37P-hTERT cells and could be a contributing factor to the abnormal growth observed. On the other hand, the effect of hNaa10 on cyclin D1 expression (55) as well as the interaction with TSC2 (53), both observed in cancer cells, was not affected in the Ogden syndrome fibroblasts. In contrast to the cell proliferation studies, viability assays demonstrated that S37P-hTERT cells have increased cellular metabolism when kept at high cell densities. When cultivated in dense cultures, S37P-hTERT cells appeared to grow on top of each other and in a less-polarized and more disorganized cell-sheets when compared with wild-type cells, a growth pattern reminiscent to the growth pattern of cancer cells for which cell–cell contact inhibition is lost (63,64). In agreement with this observation, we observed that a substantial fraction of the S37P-hTERT cells did not enter the G0 phase when kept at a high density while control cells were predominantly in the G0 phase. The very first study on Naa10 in yeast reported that Naa10 deficient cells are unable to enter the G0 phase, do not respond to the mating pheromone α-factor and are unable to sporulate which was attributed to a potential role of Naa10 in switching between the mitotic cell cycle and different cell fates (31). Also, the fact that S37P-hTERT cells are more sensitive toward stress agrees with these findings. Cell cycle arrest is crucial for cell differentiation and determining cell fate. Failure of cells to enter the stationary phase might lead to developmental defects as tissue organization is known to require strict control of cell divisions. This partial inability of

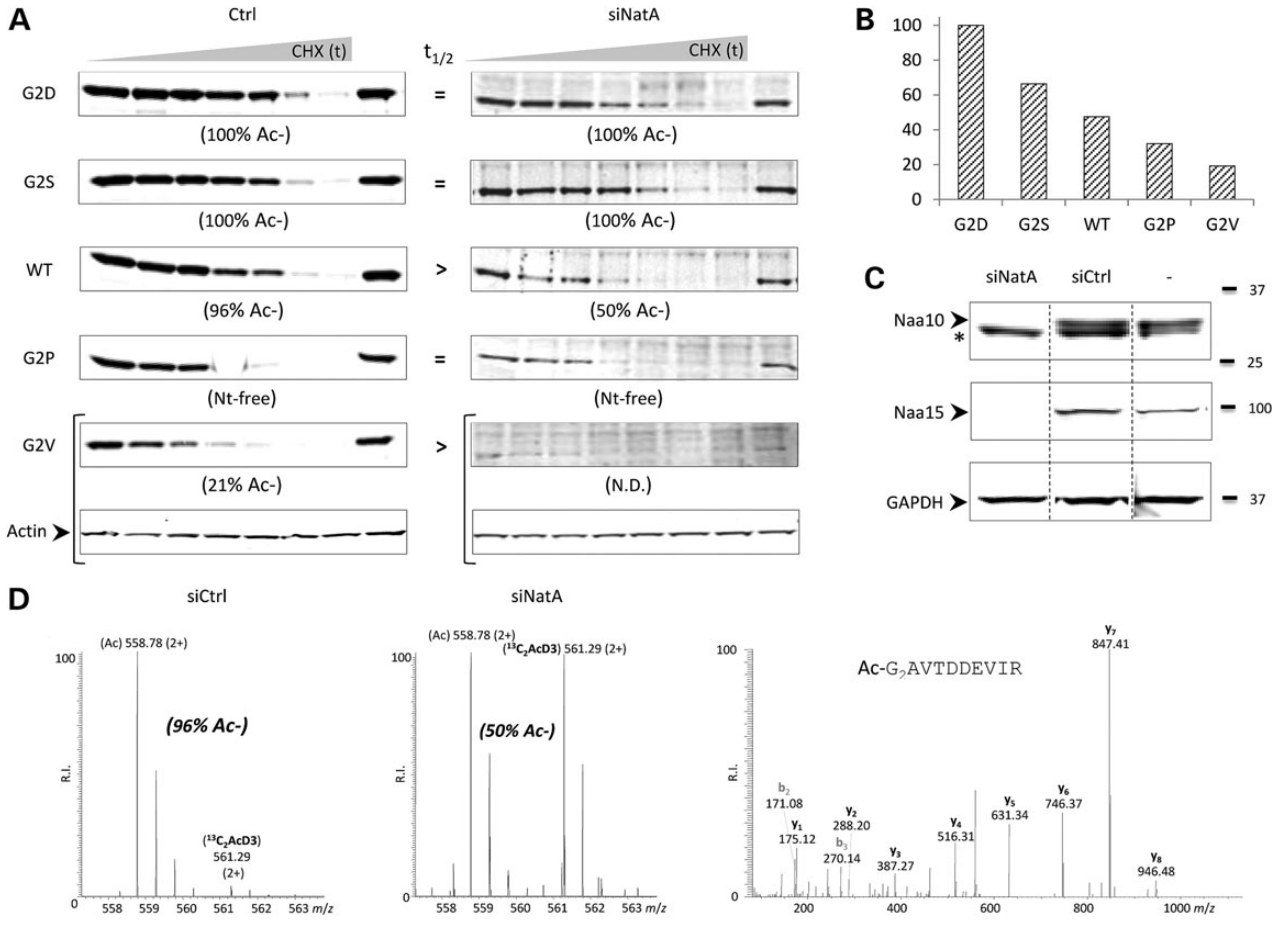

Figure 9. Reduced Nt-acetylation of THOC7 leads to a decreased protein half-life. (**A**) THOC7-V5/HIS variants were expressed in untreated and siNatA-treated A431 cells and a cycloheximide chase was performed for 15 min, 30 min, 1 h, 2 h, 4 h and 6 h. THOC7 variants were detected by means of western blotting using anti-V5 antibodies and subjected to ISIL in order to measure their Nt-acetylation status. Actin was used as control for equal protein loading. In the Y-axis, the value of 100 corresponds with a protein half-life of 1.5 h for the longest-lived THOC7 variant; THOC7-G2D as determined by densitometric analyses (**B**) shows the quantification of the protein half-life in the control cells while (**C**) shows a western blot to demonstrate efficient knockdown of hNaa10 and hNaa15 (siNatA) in A431 cells using siNatA mediated knockdown. GAPDH was used as a control for protein loading. A combined CID/HCD MS/MS spectrum of the Nt-acetylated N terminus of THOC7-WT is shown with b and y fragment ions indicated in (**D**). The CID spectrum was used for identification of the peptide (G_2AVTDDEVIR$_{11}$) and was acquired during the acquisition of the HCD spectrum of the same precursor.

S37P-hTERT cells to enter G0 phase might contribute to the developmental defects observed for Ogden syndrome males.

We also observed that S37P-hTERT cells migrate at significantly reduced speed compared with wild-type cells, especially under nutrient-starved conditions. hNaa10 has previously been shown to negatively regulate cellular motility in cancer cells by binding and inhibiting the translocation of PIX to the cell migration machinery at the plasma membrane in an acetyltransferase-independent manner (54). However, we were not able to confirm the PIX–hNaa10 interaction in either Naa10-WT or Naa10-S37P fibroblasts. hNaa10 has also been shown to regulate cell motility by inhibiting MYLK either directly through interaction or indirectly through acetylation of lysine residues on MYLK (51). We were unable to show a direct interaction between MYLK and hNaa10 in these fibroblasts. Cellular motility is critical for normal development (65) and a functional Naa10 is important as demonstrated by the partially rescued migration phenotype when overexpressing Naa10-WT in S37P-hTERT fibroblasts. We thus suspect that a reduced cell migration capacity in combination with reduced cell proliferation and loss of correct cell cycle progression may contribute to the Ogden syndrome at the cellular level.

Our structural modelling data based on the NatA crystal structure of *S. pombe* (23) revealed that the hNaa10-S37P mutation results in shortening of helix α2 thereby introducing changes in the flexibility of hNaa10 that may decrease its catalytic properties both in its NatA- or non-complexed form. Further, the changes in flexibility as well as rearrangement of hydrogen bonds in the interface between hNaa10 and the auxiliary subunit of the NatA complex, hNaa15, suggested a reduced NatA-complex stability. These hypotheses were confirmed by *in vitro* enzyme assays demonstrating a reduced enzymatic activity for both hNatA-S37P and hNaa10-S37P, likely caused by a reduced substrate peptide binding or release. Immunoprecipitation experiments revealed that NatA-complex formation was clearly impaired in S37P-hTERT cells. Our recently developed Ogden syndrome heterologous yeast model also presented data in line with these findings in terms of a reduced catalytic activity and a reduced ability to form an NatA complex when co-expressed with hNaa15 in yeast for hNaa10-S37P (37).

Steady-state protein levels of hNaa10, hNaa15 and hNaa50 in B cells from various family members including Ogden syndrome males, carrier females and unaffected individuals revealed no major differences in protein levels. This indicates that reduced

complex formation does not influence the steady-state protein levels of hNaa10 or hNaa15. In contrast, hNaa10 level seems to depend on complex formation with hNaa15 in cancer cells lines (66). Fluorescence microscopy studies demonstrated that the hNaa10-S37P mutation did not influence the subcellular localization of hNaa10 or hNaa15. Both hNaa10-WT and hNaa10-S37P were cytosolic, in contrast to what has been described in cancer and other cell lines previously, where hNaa10 is both localized to and performs functions in cytosol and nucleus (21). The bulk of the evidence shows that hNaa10 mainly performs cytosolic functions in normal cells, suggesting that Ogden syndrome is caused by an impaired cytosolic function of hNaa10-S37P, most likely involving co-translational Nt-acetylation. Indeed, N-terminal COFRADIC analysis of WT and hNaa10-S37P fibroblasts and B-cells revealed a significantly reduced degree of Nt-acetylation of certain NatA/NatE-type substrate N termini in Naa10-S37P cells. Again, this is in agreement with the abovementioned Ogden syndrome yeast model; yeast cells expressing mutant hNatA displayed a reduced degree of Nt-acetylation among a large group of NatA substrates when compared with yeast expressing wild-type hNatA (37).

The substantial loss of NatA-complex formation in cells expressing hNaa10-S37P in addition to the reduced catalytic activity toward classical NatA substrates appears sufficient to impact the Nt-acetylome. The impairment of *in vivo* NAT activity in hNaa10-S37P cells toward classical NatA substrates is clearly reflected in the COFRADIC datasets of B cells and fibroblasts from the Ogden-affected males. Here, mostly, NatA-type substrate N-termini displayed a reduced degree of Nt-acetylation, which is strongly reminiscent to the observations made in a previous NatA knockdown study (1). Several of the specific NatA substrates previously identified by means of siNatA knockdown were also identified here. The *in vitro* enzyme assays suggest that hNaa10-S37P has a decreased catalytic activity both for classical NatA substrates (Ser-, Ala-, etc.) and acidic N termini (Glu-, Asp-), the latter posttranslationally acetylated by monomeric hNaa10. However, mainly, classical NatA substrates were found to be affected in their degree of Nt-acetylation in our proteomic analyses *in vivo*. Earlier studies have suggested that primarily suboptimal substrates are affected by NatA or NatB knockdown, leaving the most preferred substrates unaffected in their Nt-acetylation states (1,56). Furthermore, as described previously, hNaa10 was also found in non-polysomal fractions in a monomeric form, indicating that it might function outside the NatA complex (28). This, together with our finding that the S37P mutation affects NatA-complex formation, indicating increased monomeric hNaa10-S37P availability, could counteract hNaa10's putatively reduced activity toward acidic N termini. We therefore hypothesize that Ogden syndrome is mainly caused by loss of NatA activity, and not by loss of NatA-independent hNaa10 activities such as the posttranslational Nt-acetylation of actin (28). A small subset of the affected N termini in the COFRADIC datasets represents non-NatA-type substrates and rather hints to NatE substrates. This is consistent with the immunoprecipitation results showing that there is less mutant hNaa10 interacting with hNaa15 and hNaa50 (NatE), although it is not clear if there is direct or indirect binding of hNaa50 to hNaa15 and/or hNaa10.

Several of the S37P-affected substrate N termini here identified by means of positional proteomics were chosen for further *in depth* analyses as they displayed an overall Nt-acetylation reduction between 10 and 40%. No observable changes in steady-state protein levels could be observed for six of the seven candidates tested. For THOC7, however, which is a component of the THO complex (67,68), a multi-protein complex implicated in the coupling of transcription and mRNA processing, a decrease in protein half-life could be observed. Here, the observed proteasomal-dependent decrease in protein half-life of THOC7 correlated with decreased Nt-acetylation, suggesting that the acetyl group confers stability to THOC7.

In conclusion, we present data supporting our hypothesis that a major contributing factor to Ogden syndrome is loss of Nt-acetylation of specific NatA- and NatE-type substrates due to reduced catalytic activity, reduced NatA-complex formation, and reduced interaction with hNaa50. Our cellular studies suggest that S37P-hTERT cells have reduced cell proliferation via perturbation of the Rb1-pathway and are dysregulated in terms of cell–cell contact inhibition and migration, possibly accounting for the detrimental effect of hNaa10-S37P observed in males suffering from Ogden syndrome.

Materials and Methods

Homology modeling

The homology model of the human NatA WT complex was built with Modeller version 9.8 (69) using the NatA complex of *S. pombe* as a template. The sequence identity between the target and the template is ~67 and 37% for the subunits Naa10 and Naa15, respectively (Supplementary Material, Fig. S1). The NatA-S37P complex was designed from the human WT NatA model using SCWRL instead of Modeller, in order to have starting structures as similar as possible as to avoid bias in comparison between the wild-type and mutant NatA complex.

MD simulations and trajectory analysis

The systems were prepared and simulated as for hNaa50 and as described by Grauffel *et al.* (41), with some differences due mostly to the size of the systems. Briefly (see details in Supplementary Material), the complexes were solvated in larger cubic boxes (120 Å-long edges). We ran long simulations (100 ns) at a temperature of 300 K using the NAMD program (70) and the CHARMM27 force field (61). The system was subjected to energy minimization, followed by a gradual heating and by a 1 ns equilibration phase during which velocities were reassigned every picosecond. The production phase consisted of a 100 ns simulation in the NPT ensemble, with a time step of 1 fs. Two simulations (replicas) using a different set of initial velocities were conducted for each system.

An extensive study of the interactions between the two subunits was conducted by using free energy decompositions and by monitoring intermolecular hydrogen bonds. All analyses were performed on the last 80 ns of simulation. They were subsequently divided into four windows of 20 ns each. Hydrogen bonds were defined using a 2.4 Å distance criterion between hydrogen and acceptor, and a 130° donor–hydrogen–acceptor angle criterion. For the analysis of atomic fluctuations, the main 20 ns long analysis windows were divided into 40 windows. Fluctuations were computed on each of these 500 ps windows using the corresponding average structure. Fluctuations are considered different when two or more consecutive residues have an increase or decrease of fluctuations >10%. The protocol used to obtain the energetic contributions of all amino acids to the formation of the complexes is based on the MM/PBSA approach (71). Briefly, 25 representative conformations are extracted at regular intervals from 20 ns-long segments of the trajectory. Van der Waals interactions and non-polar contributions are evaluated with CHARMM using Lennard-Jones potential and solvent

accessible surface area analysis, respectively. Electrostatics is evaluated using the program UHBD (72). These decompositions are performed at the backbone/side chain level in order to get more insights into interactions. The reported binding energies are averages over eight 20 ns-long segments.

Sample collection

The sample collection for blood (B cells), fibroblasts and cell line creation was approved by the institutional review board at the University of Utah. Written informed consent was obtained from the Ogden syndrome family for all sample collections. Deidentified aliquots of cell lines were distributed for use in the experiments described.

Materials and antibodies

Antibodies used in this study were anti-hNaa10 (anti-hARD1) (21), anti-hNaa15 (anti-NATH) (21), anti-hNaa50 (Biogenes, custom-made rabbit IgG toward amino acid 150–163 of hNaa50), rabbit anti-Naa50 (LifeSpan BioSciences, #LS-C81324-100), anti-V5 (Life Technologies; R960-25), anti-Myc (Life Technologies; R950-25), anti-tuberin (TSC2, Santa Cruz Biotechnologies; sc-893), anti-β-PIX (ARHGEF7, Santa Cruz Biotechnologies; sc-10932), anti-MYLK (Santa Cruz Biotechnologies; sc-9452), anti-pS6K1 (phosphoThr389, Cell Signaling; 9234), anti-Rb (Cell Signaling; 9309), anti-Cyclin E2 (Cell Signaling; 4132), anti-p21(p21(SX118) Cip1, Santa Cruz Biotechnologies; sc-53870), anti-p27 (p27Kip1, Santa Cruz Biotechnologies; sc-53871, anti-β-tubulin (Sigma-Aldrich; T5293), anti-GAPDH (Santa Cruz; sc-25778, Abcam; Ab 8245) and anti-actin (Santa Cruz Biotechnologies; SC1615, Sigma-Aldrich; A2066). The secondary antibodies used for western blot visualization of the primary antibodies were HRP-linked sheep anti-mouse, sheep anti-rabbit (GE Healthcare; NXA931), donkey anti-rabbit (GE Healthcare; NA934V) and mouse anti-goat (Santa Cruz Biotechnologies; sc-2354) antibodies next to the infrared dye coupled antibodies; IRDye 800 CW goat anti-rabbit IgG (Westburg, LI-COR; 926-32211), IRDye 680 CW goat anti-rabbit IgG (Westburg, LI-COR; 926-32221) or IRDye 680 CW goat anti-mouse antibody IgG (Westburg, LI-COR; 926-32220) and IRDye 800 CW goat anti-mouse antibody IgG (Westburg, LI-COR; 926-32210) as indicated in the figures and method text.

Cell culture, virus production and cell treatment

Primary B cells were isolated from Ogden patients, EBV immortalized at the University of Utah core facility, and cultured in HyClone Roswell Park Memorial Institute 1640 supplemented with 15% fetal calf serum and 3% L-glutamine. Primary BJ cells [American type culture collection (ATCC), CRL-2522], isolated from newborn male foreskin, primary dermal fibroblasts, neonatal (HDFn; Life Technologies; C-004-5C) and primary S37P fibroblasts (III-6) from a skin-punch biopsy, isolated at the University of Utah were cultured in Eagle's minimal essential medium (EMEM) supplemented with 10% fetal bovine serum (FBS) and 3% L-glutamine. 293T (Phoenix amphotropic, ATCC; CRL-3213) and HeLa (ATCC; CCL-2) cells were maintained in Dulbecco's modified Eagle's medium (DMEM) supplemented with 10% FBS and 3% L-glutamine. Human A431 cells (epidermoid carcinoma; ATCC; CRL1555) were cultured in Glutamax-containing DMEM supplemented with 10% dialyzed FBS (Invitrogen), 100 units/ml penicillin (Invitrogen) and 100 µg/ml streptomycin (Invitrogen). Cells were cultured at 37°C in a humidified atmosphere with 5% CO_2.

Replication defective virus was produced by transfecting 293T cells with pMIGR1-hTERT and pCMV-VSVG and harvested 48 h posttransfection at 500 *g* for 5 min. The virus suspension was filtered through a 0.45 µm filter before 5 µg/ml protamine sulfate was added. Primary fibroblasts (BJ and S37P) were infected with virus representing hTERT for 12 h before supernatant was removed and cells washed with phosphate-buffered saline (PBS) and culture medium. The cells were cultured for at least 10 days and two cell cultivations before hTERT- (GFP) positive cells were sorted by FACS by use of FACS Aria.

To inhibit proteasomal-mediated degradation of expressed proteins, 5 µM MG132 (Calbiochem; 4747490) was added to transiently transfected cells for the indicated time-points before lysis. To inhibit protein synthesis and study stability of expressed proteins a chase with 50 µg/ml cycloheximide (Sigma-Aldrich; C6255) was performed for 15 min, 30 min, 1 h, 2 h, 4 h and 6 h. After drug treatment, cell lysates were prepared and analyzed by western blotting as described below.

X-chromosome skewing assay

The X-inactivation pattern of female mutation carriers and non-carriers from the Utah family was determined by analyzing the methylation sites in the first exon of the human androgen receptor locus as described previously (73). Briefly, genomic DNA was isolated from leucocytes and PCR with gene-specific and fluorescently labeled primers was performed. Digested and undigested products were analyzed by capillary electrophoresis and peak areas were determined to quantify the skewing patterns. All experiments were performed at least in duplicate and results were averaged.

Since this assay is quantitative but does not provide information which Naa10 allele is inactivated, an *NAA10* mutation-specific X-inactivation assay was performed. For this assay, 375 ng of genomic DNA from each of four female carriers of the c.109T > C (p.S37P) mutation and two wild-type females was digested in a 10 µl volume with the methylation-sensitive restriction endonuclease *Sma*I (New England BioLabs) for 3 h at 25°C, followed by heat inactivation at 65°C for 30 min. Primers were designed to amplify a 653 bp PCR product that encompassed the c.109T > C (p.S37P) mutation in exon 2 of NAA10 and an *Sma*I site (chrX:153200324-153200329 [hg19]) in an adjacent CpG island (forward: GCAGCTGACTGCGCCTTCAC; reverse: TCCCTCCAA GATGGCCAGATG). PCR was performed in a 10 µl volume using the FailSafe™ PCR System and PreMix J (Epicentre® [an Illumina® company]) with 2 µl of uncleaned, digested DNA as template. The reactions were denatured at 94°C for 1 min, then 35 cycles of 94°C for 15 s, 62°C for 10 s and 72°C for 1 min were performed. Sanger sequencing of the amplified products was completed using standard methods. Since the PCR product does not amplify from DNA that has been cut by *Sma*I (unmethylated DNA), skewed X-inactivation is seen as apparent loss of heterozygosity of the p.S37P mutation and other variants within the sequenced amplicon.

Immunoblotting

B cells and fibroblasts were harvested, washed two times in cold PBS and lysed by incubation in IPH lysis buffer (50 mM Tris–HCl, pH 8.0, 0.5% Nonidet P-40, 5 mM EDTA and EDTA-free protease inhibitor) on ice for 15 min. Cellular debris was pelleted at 15 700*g* for 1 min. Sample-loading buffer was added to the lysate supernatant and proteins were separated by SDS–PAGE using Tris-glycine or polyacrylamide Criterion XT-gels (Bio-Rad). Subsequently, proteins were transferred onto a nitrocellulose or PVDF membrane. Membranes were blocked with 5% non-fat

dry-milk (Regilait) or 1 : 1 Tris-buffered saline and 0.1% Tween-20 (TBS-T) Odyssey Blocking solution (LI-COR; 927-40003) before incubation with antibodies as mentioned in Materials and antibodies. Bands were visualized using a ChemiDoc™ XRS+ and ImageLab v3.0 or Odyssey infrared imaging system (LI-COR).

Immunofluorescence assay

Fibroblasts cultured on coverslips were washed in cytoskeleton buffer (134 mM NaCl, 5 mM KCL, 1.1 mM $Na_2HPO_2{\cdot}2H_2O$, 0.4 mM KH_2PO_4, 5.5 mM glucose, 4 mM $NaHCO_3$, 10 mM MES, pH 6.1, 2 mM EGTA, 2 mM $MgCl_2$) and fixed with 4% paraformaldehyde. Cells were permeabilized in 0.1% Triton X-100 and blocked in 1–10% BSA before the proteins of interest were labeled with the indicated primary antibodies. Secondary antibodies used were Alexa Fluor 488 or 594. Micrographs were acquired using a Leica TCS SP5 multiphoton confocal microscopy. Z-stacks and Z-stack projections were handled using Fiji Image Processing Software.

Protein expression and purification

Plasmids-encoding recombinant His-tagged MBP-hNaa10-WT and MBP-hNaa10-S37P were transformed into *E. coli* BL21 star (DE3) cells by heat shock transformation, and grown in 200 ml cultures to an $OD_{600\ nm}$ of 0.6. Cell cultures were cooled down to 16°C and protein expression was induced by adding 1 mM of IPTG. Cell cultures were incubated for 14 h, harvested in 100 ml pellets and stored at −20°C. Pellets were dissolved in lysis buffer (50 mM Tris–HCl, pH 7.4, 300 mM NaCl, 2 mM DTT and EDTA-free protease inhibitor) and cells lysed in a French press. Cell debris was removed by centrifugation at 17 000 *g* at 4°C for 20 min. Recombinant proteins were purified by Immobilized Metal Affinity Chromatography and size-exclusion chromatography (Superdex 200 10/300). Fractions were analyzed by SDS–PAGE, and protein concentrations determined by OD_{280} measurements (Nanodrop1000) and Bradford assay (Bio-Rad).

Quantitative *in vitro* acetylation assay and determination of kinetic constants

Purified recombinant MBP-tagged enzymes were mixed with Acetyl-CoA (10–500 μM) and synthetic oligopeptides (10–1000 μM) and incubated in acetylation buffer (50 mM Tris–HCl, pH 8.5, 1 mM EDTA, 10% glycerol) for 10 min at 37°C. Reactions were stopped by adding a final concentration of 1% trifluoroacetic acid (TFA) to the mixture. Peptides were custom-made (Biogenes) to a purity of 80–95%. All peptides (24-mers) contain seven unique amino acids at their N-terminus, as these harbor the major substrate determinants influencing N-terminal acetylation. The next 17 amino acids are essentially identical to the ACTH peptide sequence (RWGRPVGRRRR PVRVYP); however, lysines were replaced by arginines to minimize any potential interference by N^{ε}-acetylation. The following synthetic oligopeptides were used: the N terminus of SMCA4: ([NH2]STPDPPLRWGRPVGRRRRPVRVYP[OH]), the N terminus of RNaseP protein p30: ([NH2]AVFADLDRWGRPVGRRRRPVRVYP[OH]) both representing "classical" *in vivo* NatA substrates and the N terminus of γ-actin: ([NH2]EEEIAALRWGRPVGRRRRPVRVYP [OH]).

Immunoprecipitation of hNatA and acetylation assay from fibroblasts

Approximately 1–3 × 10^7 fibroblasts were harvested, washed in cold PBS and lysed by incubation in 500 μl IPH lysis buffer on ice for 15 min. Cell lysates were centrifuged at 15 700*g* for 5 min and the supernatant collected. Fifty microliters of magnetic Protein A/G-Agarose slurry (Thermo Scientific; 88 803) were added to the supernatant and incubated for 2 h for pre-clearing the lysate. The magnetic beads were removed and 15 μg anti-hNaa15 was added to the supernatant and incubated for 2 h before 50 μl magnetic Protein A/G-Agarose slurry was added and incubated for 16 h at 4°C. In each case, the magnetic Protein A/G-Agarose beads were washed three times in cold lysis buffer and two times in acetylation buffer. The amount of enzyme present in each sample was determined by western blotting and densitometry analysis by the use of ImageLab v3.0 with antibodies against hNaa10 and hNaa15. The measured enzyme activity was adjusted according to hNaa15-levels or hNaa10-levels present in the immunoprecipitates.

To analyze the interaction of exogenously expressed hNaa10 and hNaa15, 8 × 10^5 HEK293 cells were seeded in 6-well plates and incubated at 37°C for 24 h. Cells were transiently transfected with 2 μg pcDNA3.1/V5-His hNaa10-WT, pcDNA3.1/V5-His hNaa10-S37P, pcDNA3.1/Myc-His hNaa15-WT and/or empty control vectors. Cells were lysed 48 h posttransfection in 200 μl lysis buffer (PBS, 0.2%, v/v, Triton X-100, complete protease inhibitor cocktail (Roche)). Cellular debris was pelleted at 20 800 *g* for 10 min at 4°C. The protein concentration was determined using advanced protein assay (Cytoskeleton, Inc.) and 600–800 μg total protein was used for IP. Cell lysates were incubated with 1 μg anti-V5 or anti-Myc antibody for 1 h under constant agitation at 4°C. Immune complexes were precipitated with 30 μl 1 : 1 slurry Protein-A sepharose (Invitrogen) for 30 min at 4°C. Beads were pelleted by centrifugation at 2700 *g* for 2 min, washed three times with 300 μl lysis buffer and protein complexes were eluted with 50 μl 2× SDS-sample buffer and analyzed by SDS–PAGE and western blotting.

Creation of eukaryotic expression plasmids using gateway cloning

pOTB7 and pCMV-SPORT6 vectors (THOC7: cat n° IRATp970D0486D, SAE1: cat n° IRATp970D0613D, OTU7B: cat n° IRATp970D03105D; ELOA1: cat n° IRAUp969E1025D; RL13A: IRAUp969D105D, RZPD Imagenes) served as templates to generate attB-flanked PCR products of WT constructs next to a series of N-terminal mutants where the second amino acid was replaced to Ser, Val, Pro or Asp. These PCR products were suitable for use in a Gateway® BP recombination reaction with a donor vector (pDONR221, Invitrogen; 12536–017) thereby creating an entry clone. The reverse primers were designed to fuse the desired PCR products in frame with a C-terminal V5/His-tag. To create the expression constructs, the cDNA inserts of the entry clones were shuttled into the pEF-DEST51 destination vector (Invitrogen; 12285-011) using LR-clonase recombination (Invitrogen; 11791-020) according to the manufacturer's instructions. The correctness of all cDNA sequences generated was confirmed by DNA-sequencing. All constructs were C-terminally V5-/His tagged. Transient transfections of A431 cells were performed and cells were treated with the proteasomal inhibitor MG132 or treated with the translation inhibitor cycloheximide. The tagged proteins were detected by means of western blotting using anti-V5 antibodies or subjected to immunoprecipitation coupled to ISIL for downstream mass spectrometry-based analyses of their Nt-acetylation status (30,62).

Transfection of constructs encoding N-terminal variants of hNaa10-S37P-affected substrates

A431 cells, seeded 1 day prior to transfection at 12 × 10^4 cells/well in a 12-well plate, were transfected for 24 h with 0.8 μg of eukaryotic expression vector or co-transfected for 24 h with 0.4 μg of eukaryotic expression vector and 0.4 μg pEF/GW-51/lacZ (served as

an internal control of transfections efficiency) (Invitrogen; 12 285 011) using Fugene HD (Roche; 04 709 705 001) according to the manufacturer's instructions. 24 h after transfection, cells were lysed on plate in 100 µl RIPA lysis buffer (50 mM Tris–HCl, pH 7.8, 150 mM NaCl, 1% NP-40 and protease inhibitor cocktail tablet; Roche, 11 697 498 001), subjected to freeze–thaw lysis and centrifuged for 10 min at 16 000*g*. Sample-loading buffer was added to the lysate supernatant and protein expression was analyzed by western blotting as described previously.

Immunoprecipitation of overexpressed THOC7 variants

A431 cells were harvested and lysed in RIPA lysis buffer. Anti-V5 Antibody (Invitrogen, R960-25), diluted in PBS (pH 7.4) and 0.01% Tween-20, was bound to magnetic protein G Dynabeads® beads (Invitrogen; 1003D) at a ratio of 2 µg antibody per 15 µl beads in 100 µl PBS-Tween for 30 min at room temperature. Unbound antibody was removed and the antibody bound beads were washed with PBS-Tween before addition of the cell lysate. Three hundred and fifty micrograms of protein lysate were added to 15 µl antibody bound beads and incubated overnight at 4°C on a rotator. Following incubation, three repetitive rounds of supernatant removal and washing in PBS-Tween were performed. Finally, the immunoprecipitates were eluted with elution buffer (sample-loading buffer in 50 mM Tris–HCl, pH 8.0) by heating for 10 min at 95°C and analyzed by western blotting and by ISIL followed by in-gel digestion for the determination of their Nt-acetylation states (62).

Determination of the Nt-acetylation status using ISIL followed by in-gel digestion

siCtrl and siNatA knockdown cell lysates were prepared as described above and the samples were analyzed on a 4–16% gradient XT precast Criterion gel using XT-MOPS buffer (Bio-Rad). Gel slices corresponding to the molecular weights (~29 kDa) of the tagged THOC7 variants (between 25 and 37 kDa) were cut from the gel and ISIL was performed as described previously (62). The resulting peptide mixtures were acidified (0.1% formic acid) and analyzed by LC–MS/MS analysis. Peptide mixtures were introduced into an Ultimate 3000 RSLC nano LC-MS/MS system (Dionex, Amsterdam, The Netherlands) in-line connected to an LTQ Orbitrap Velos (Thermo Fisher Scientific, Bremen, Germany) as described previously (30). When operating the instrument in Higher Energy Collision Dissociation (HCD), spectra were acquired in the Orbitrap with an effective FWHM resolution >7500 around *m/z* 400. The extent of Nt-acetylation was calculated from the peptide ion signals observed in the MS spectra (5).

NatA knockdown and THOC7 transgene expression

siRNA transfections were performed using HiPerFect (Qiagen) and 20 nM si-non-targeting control (Dharmacon; D-001810-10) or a pool of 10 nM sihNAA10 (Dharmacon, SMARTpool siGENOME NAA10 siRNA; M-009606-00-0005) and 10 nM sihNAA15 (custom oligonucleotide, GGGACCUUUCCUUACUACAdTdT). For the siRNA transfections, 2.5×10^5 A431 cells were seeded in 6-well plated and reverse transfected. During the time-course of the experiment, the pan-caspase inhibitor zVAD-fmk was added to the cells to a final concentration of 10 µM and replenished after each transfection step. Cells were re-transfected under the same conditions 48 h after the first transfection. At 72 h, the cells were transiently transfected for 24 h with the eukaryotic THOC7 expression constructs using Fugene HD (as described above). At 96 h, cells were subjected to a CHX chase for 15 min, 30 min, 1 h, 2 h, 4 h and 6 h and harvested (as described above). Cell lysates were analyzed by western blotting.

N-Terminal COFRADIC, LC–MS/MS analysis and data storage

N-Terminal COFRADIC analyses were performed as described previously (74). To enable the assignment of *in vivo* Nt-acetylation events, all primary protein amines were blocked making use of (stable isotopic encoded) an *N*-hydroxysuccinimide ester at the protein level (i.e. NHS ester of $^{13}C_2D_{3)}$. The obtained peptide mixtures were introduced into an LC–MS/MS system, the Ultimate 3000 (Dionex, Amsterdam, The Netherlands) in-line connected to an LTQ Orbitrap XL mass spectrometer (Thermo Fisher Scientific) and LC–MS/MS analysis was performed as described previously (1,5). The generated MS/MS peak lists were searched with Mascot using the Mascot Daemon interface (version 2.2.0, Matrix Science). Searches were performed in the Swiss-Prot database with taxonomy set to human. $^{13}C_2D_3$-acetylation of lysine side chains, carbamidomethylation of cysteine and methionine oxidation to methionine-sulfoxide were set as fixed modifications for the N-terminal COFRADIC analyses. Variable modifications were $^{13}C_2D_3$-acetylation and acetylation of protein N termini. Pyroglutamate formation of N-terminal glutamine was additionally set as a variable modification. For the differential N-terminal COFRADIC analyses performed (fibroblast samples), a $^{12}C_6$ L-arginine versus $^{13}C_6^{15}N_4$ L-arginine quantification option was additionally selected for identification and quantification, and carried out using the Mascot Distiller Quantitation Tool (version 2.2.1). Mass tolerance on precursor ions was set to 10 ppm (with Mascot's C13 option set to 1) and on fragment ions to 0.5 Da. Endoproteinase semi-Arg-C/P (Arg-C specificity with arginine–proline cleavage allowed) was set as enzyme allowing no missed cleavages. The peptide charge was set to 1+, 2+, 3+ and instrument setting was put to ESI-TRAP. Only peptides that were ranked 1 and scored above the threshold score, set at 99% confidence, were withheld. Quantification of the degree of Nt-acetylation was performed as described previously (5). In all cases, two isotopic envelopes could clearly be distinguished [i.e. those of the *in vivo* acetylated (Ac) and *in vitro* acetylated forms ($^{13}C_2D_3$)]. All data management were done in ms_lims (75). The mass spectrometry proteomics data have been deposited to the ProteomeXchange Consortium (http://proteomecentral.proteomexchange.org) via the PRIDE partner repository with the dataset identifier PXD000551 and 10.6019/PXD000551 and PRIDE accessions 31944–31957 for the B cells and the dataset identifier PXD001282 and 10.6019/PXD001282 for the fibroblasts.

Metabolic SILAC of fibroblasts

Primary and immortalized fibroblasts were cultured in MEM SILAC growth medium supplemented with 10% dialyzed FBS and either natural $^{12}C_6$-L-arginine (Sigma-Aldrich; A8094) for BJ control cells (WT or WT-hTERT cells) or $^{13}C_6^{15}N_4$-L-arginine (Sigma-Aldrich; 608033) for hNaa10-S37P cells (S37P or S37P-hTERT cells) at a concentration of 37.8 mg/l (i.e. 30% of the suggested concentration present in EMEM at which arginine to proline conversion was not detectable for S37P fibroblasts). Cells were cultured for at least six population doublings (14 days) to ensure complete incorporation of the labeled arginine. All free N termini were *in vitro* labeled by $^{13}C_2D_3$-acetylation and this labeling combined with differential L-arginine SILAC allows for the calculation of the degree of Nt-acetylation and for the relative quantification of N-terminal peptides between two samples (5,56,60). Cells

($1–3 \times 10^7$) were lysed in 50 mM sodium phosphate (pH 7.5), 100 mM NaCl, 1% CHAPS, 0.5 mM EDTA and 0.5 × complete protease inhibitor cocktail (Roche) for 15 min one ice and centrifuged for 3 min at 16 000 *g* at 4°C, protein concentrations measured and equal amounts of control and S37P cell lysate mixed together before the lysates were subjected to N-terminal COFRADIC analysis and LC–MS/MS analysis as previously described (74).

Cell proliferation and WST-8 metabolic activity

The proliferation and cell counting assay was performed by seeding 65 000 WT- and S37P-hTERT fibroblasts into a 6 cm Nunc dish and the cells counted 1 week later. All cell seeding density proliferation assays were performed at least in triplicate. Primary fibroblasts, 2×10^4, HDFn (hNaa10-WT) and one Ogden boy (S37P; III-6), at Passage 4 were plated in each well of two 12-well plates, and left overnight to adhere. The cells were harvested and counted every day for 7 days.

For the WST-8 assay, WT- and S37P-hTERT fibroblasts were counted and seeded into 96-well plates with 1000, 5000 or 10 000 cells/well. Cell counting was done with the TC10^{tm} Automated Cell Counter. Cell medium was changed every 24 h. Five days later, the cells were incubated with CCVK-1 solution in a 1/100 dilution in cell medium. After 1 h incubation, the absorbance was measured at 450 nm with an Epoch Microplate Spectrophotometer. This was done according to the manufacturer's instructions (Colometric Cell Viability Kit I, cat.no PK-CA705-CK04, PromoKine) and absorbance measured at 450 nm with an Epoch Microplate Spectrophotometer. The increase in cell viability was expressed as the ratio of absorbance (S37P-hTERT) versus absorbance (WT-hTERT) multiplied by 100 [(abs S37P-hTERT/abs WT-hTERT) × 100]. The absorbance of WT-hTERT was assumed to represent 100% viability. The data for quantification of the cell viability of WT- and S37P-hTERT are shown as the mean of at least three independent experiments, each with at least three technical replicates for each measurement. The *P*-values were calculated using paired *t*-tests.

BrdU cell proliferation assay of primary fibroblasts

Primary hNaa10-WT fibroblasts (HDFn), 5×10^4 and one Ogden boy (S37P; III-6) at passage 4 were plated in 12-well plates on glass coverslips coated with matrigel (Corning; 354230). To measure BrdU incorporation, the cells were incubated for 5 h with BrdU label (Millipore; QIA58, 1 : 2000) at 46 h after seeding, then fixed with 3.7% paraformaldehyde for 15 min at room temperature, washed in PBS, treated with 0.07 N NaOH for 15 min at room temperature, and blocked in 10% goat serum, 1% BSA and 0.3% Triton X-100 for 15 min at room temperature before staining. The cells were then stained with a BrdU antibody (1 : 100) for 1 h at room temperature, washed and incubated with secondary antibody (AlexaFluor goat anti-mouse 488, Life Technologies; A-11029, 1 : 1000) for 1 h at room temperature. Hoechst 33 342 was used as a nuclear stain (Molecular Probes, Life Technologies; R37605). Quantitative analysis was performed by counting, for each cell types, the percentage of BrdU-positive nuclei on a total of ~1000 cells, randomly observed in 15 microscopic fields from WT fibroblasts and 22 microscopic fields from S37P fibroblasts.

Wound-healing (migration) assay

Fibroblasts were cultivated to a high density in wells of culture inserts (Ibidi) for live cell analysis. Culture inserts were removed at time 0 indicating that the start of the cell migration/wound-healing assay and growth medium was replaced either with new medium containing FBS and L-glutamine or L-glutamine containing medium without FBS or with media without both FBS and L-glutamine. Pictures were taken every 15 min for 48 h and a time-lapse video was generated by 10 pictures/s.

Cell cycle analysis

Fibroblasts were washed, harvested by trypsination and cells counted. Equal amount of cells ($\geq 3 \times 10^6$ cells) were fixed with 70% ethanol at 4°C overnight. Cells were washed with 1× PBS before treatment with heat-activated RNase A (300 µg/µl) at 37°C for 30 min followed by propidium staining (300 µg/µl) for 5 min and two washes. Samples were analyzed by use of BD LSR Fortessa and further processed by FlowJo.

Supplementary Material

Supplementary Material is available at *HMG* online.

Acknowledgements

The authors express their appreciation to the Ogden syndrome family for their generous cooperation, and we thank Alan Rope for assistance with the skin-punch biopsy for fibroblast collection from the Ogden syndrome boy. Heidi Fain provided technical assistance with isolation and culture of B cells. Sarah South and her team at ARUP, University of Utah, helped establishing the skin fibroblasts in culture. Bjørg Flatekvål provided technical assistance with fibroblast cultivation and western blotting.

Conflict of Interest statement. None declared.

Funding

This work was supported by the Stanley Institute for Cognitive Genomics (to G.J.L.); the Clinical Genetics Research Program: Phenotyping Core at the University of Utah (CCTS grant UL1RR025764 to G.J.L.); the Research Foundation – Flanders (FWO-Vlaanderen) (G.0440.10 to K.G., G.0269.13N to P.V.D.); the Research Council of Norway (197136 and 230865 to T.A.); the Norwegian Cancer Society (PR-2009-0222 to T.A.); the Bergen Research Foundation (BFS) (to T.A.); The Western Norway Regional Health Authority (to T.A.); the National Institutes of Health (R01 GM020693 to R.M.); and PRIME-XS (grant agreement number 262067, funded by the European Union 7th Framework Program). Funding to pay the Open Access publication charges for this article was provided by the University of Bergen.

References

1. Arnesen, T., Van Damme, P., Polevoda, B., Helsens, K., Evjenth, R., Colaert, N., Varhaug, J.E., Vandekerckhove, J., Lillehaug, J.R., Sherman, F. *et al.* (2009) Proteomics analyses reveal the evolutionary conservation and divergence of N-terminal acetyltransferases from yeast and humans. *Proc. Natl. Acad. Sci. USA*, **106**, 8157–8162.
2. Starheim, K.K., Gevaert, K. and Arnesen, T. (2012) Protein N-terminal acetyltransferases: when the start matters. *Trends Biochem. Sci.*, **37**, 152–161.
3. Goetze, S., Qeli, E., Mosimann, C., Staes, A., Gerrits, B., Roschitzki, B., Mohanty, S., Niederer, E.M., Laczko, E., Timmerman, E. *et al.* (2009) Identification and functional characterization of N-terminally acetylated proteins in Drosophila melanogaster. *PLoS Biol.*, **7**, e1000236.

4. Bienvenut, W.V., Sumpton, D., Martinez, A., Lilla, S., Espagne, C., Meinnel, T. and Giglione, C. (2012) Comparative large scale characterization of plant versus mammal proteins reveals similar and idiosyncratic N-α-acetylation features. *Mol. Cell. Proteomics*, **11**, M111.015131.
5. Van Damme, P., Hole, K., Pimenta-Marques, A., Helsens, K., Vandekerckhove, J., Martinho, R.G., Gevaert, K. and Arnesen, T. (2011) NatF contributes to an evolutionary shift in protein N-terminal acetylation and is important for normal chromosome segregation. *PLoS Genet.*, **7**, e1002169.
6. Jörnvall, H. (1975) Acetylation of protein N-terminal amino groups structural observations on α-amino acetylated proteins. *J. Theor. Biol.*, **55**, 1–12.
7. Hwang, C.-S., Shemorry, A. and Varshavsky, A. (2010) N-terminal acetylation of cellular proteins creates specific degradation signals. *Science*, **327**, 973–977.
8. Shemorry, A., Hwang, C.-S. and Varshavsky, A. (2013) Control of protein quality and stoichiometries by N-terminal acetylation and the N-end rule pathway. *Mol. Cell*, **50**, 540–551.
9. Scott, D.C., Monda, J.K., Bennett, E.J., Harper, J.W. and Schulman, B.A. (2011) N-terminal acetylation acts as an avidity enhancer within an interconnected multiprotein complex. *Science*, **334**, 674–678.
10. Holmes, W.M., Mannakee, B.K., Gutenkunst, R.N. and Serio, T. R. (2014) Loss of amino-terminal acetylation suppresses a prion phenotype by modulating global protein folding. *Nat. Commun.*, **5**, 4383.
11. Murthi, A. and Hopper, A.K. (2005) Genome-wide screen for inner nuclear membrane protein targeting in Saccharomyces cerevisiae: roles for N-acetylation and an integral membrane protein. *Genetics*, **170**, 1553–1560.
12. Behnia, R., Panic, B., Whyte, J.R. and Munro, S. (2004) Targeting of the Arf-like GTPase Arl3p to the Golgi requires N-terminal acetylation and the membrane protein Sys1p. *Nat. Cell. Biol.*, **6**, 405–413.
13. Setty, S.R.G., Strochlic, T.I., Tong, A.H.Y., Boone, C. and Burd, C.G. (2004) Golgi targeting of ARF-like GTPase Arl3p requires its N[alpha]-acetylation and the integral membrane protein Sys1p. *Nat. Cell. Biol.*, **6**, 414–419.
14. Hofmann, I. and Munro, S. (2006) An N-terminally acetylated Arf-like GTPase is localised to lysosomes and affects their motility. *J. Cell Sci.*, **119**, 1494–1503.
15. Aksnes, H., Osberg, C. and Arnesen, T. (2013) N-terminal acetylation by NatC is not a general determinant for substrate subcellular localization in Saccharomyces cerevisiae. *PLoS ONE*, **8**, e61012.
16. Forte, G.M.A., Pool, M.R. and Stirling, C.J. (2011) N-terminal acetylation inhibits protein targeting to the endoplasmic reticulum. *PLoS Biol.*, **9**, e1001073.
17. Polevoda, B., Arnesen, T. and Sherman, F. (2009) A synopsis of eukaryotic Nalpha-terminal acetyltransferases: nomenclature, subunits and substrates. *BMC Proc.*, **3**(Suppl. 6). S2.
18. Polevoda, B., Norbeck, J., Takakura, H., Blomberg, A. and Sherman, F. (1999) Identification and specificities of N-terminal acetyltransferases from Saccharomyces cerevisiae. *EMBO J.*, **18**, 6155–6168.
19. Mullen, J.R., Kayne, P.S., Moerschell, R.P., Tsunasawa, S., Gribskov, M., Colavito-Shepanski, M., Grunstein, M., Sherman, F. and Sternglanz, R. (1989) Identification and characterization of genes and mutants for an N-terminal acetyltransferase from yeast. *EMBO J.*, **8**, 2067–2075.
20. Park, E.C. and Szostak, J.W. (1992) ARD1 and NAT1 proteins form a complex that has N-terminal acetyltransferase activity. *EMBO J.*, **11**, 2087–2093.
21. Arnesen, T., Anderson, D., Baldersheim, C., Lanotte, M., Varhaug, J.E. and Lillehaug, J.R. (2005) Identification and characterization of the human ARD1-NATH protein acetyltransferase complex. *Biochem. J.*, **386**, 433–443.
22. Gautschi, M., Just, S., Mun, A., Ross, S., Rücknagel, P., Dubaquié, Y., Ehrenhofer-Murray, A. and Rospert, S. (2003) The yeast Nα-acetyltransferase NatA is quantitatively anchored to the ribosome and interacts with nascent polypeptides. *Mol. Cell. Biol.*, **23**, 7403–7414.
23. Liszczak, G., Goldberg, J.M., Foyn, H., Petersson, E.J., Arnesen, T. and Marmorstein, R. (2013) Molecular basis for N-terminal acetylation by the heterodimeric NatA complex. *Nat. Struct. Mol. Biol.*, **20**, 1098–1105.
24. Arnesen, T., Anderson, D., Torsvik, J., Halseth, H.B., Varhaug, J.E. and Lillehaug, J.R. (2006) Cloning and characterization of hNAT5/hSAN: An evolutionarily conserved component of the NatA protein N-α-acetyltransferase complex. *Gene*, **371**, 291–295.
25. Arnesen, T., Starheim, K.K., Van Damme, P., Evjenth, R., Dinh, H., Betts, M.J., Ryningen, A., Vandekerckhove, J., Gevaert, K. and Anderson, D. (2010) The chaperone-like protein HYPK acts together with NatA in cotranslational N-terminal acetylation and prevention of huntingtin aggregation. *Mol. Cell. Biol.*, **30**, 1898–1909.
26. Hou, F., Chu, C.-W., Kong, X., Yokomori, K. and Zou, H. (2007) The acetyltransferase activity of San stabilizes the mitotic cohesin at the centromeres in a shugoshin-independent manner. *J. Cell. Biol.*, **177**, 587–597.
27. Evjenth, R., Hole, K., Karlsen, O.A., Ziegler, M., Arnesen, T. and Lillehaug, J.R. (2009) Human Naa50p (Nat5/San) displays both protein Nα- and Nε-acetyltransferase activity. *J. Biol. Chem.*, **284**, 31122–31129.
28. Van Damme, P., Evjenth, R., Foyn, H., Demeyer, K., De Bock, P.-J., Lillehaug, J.R., Vandekerckhove, J., Arnesen, T. and Gevaert, K. (2011) Proteome-derived peptide libraries allow detailed analysis of the substrate specificities of Nα-acetyltransferases and point to hNaa10p as the post-translational actin Nα-acetyltransferase. *Mol. Cell. Proteomics*, **10**, M110.004580.
29. Liszczak, G., Arnesen, T. and Marmorstein, R. (2011) Structure of a ternary Naa50p (NAT5/SAN) N-terminal acetyltransferase complex reveals the molecular basis for substrate-specific acetylation. *J. Biol. Chem.*, **286**, 37002–37010.
30. Foyn, H., Van Damme, P., Støve, S.I., Glomnes, N., Evjenth, R., Gevaert, K. and Arnesen, T. (2013) Protein N-terminal acetyltransferases act as N-terminal propionyltransferases in vitro and in vivo. *Mol. Cell. Proteomics*, **12**, 42–54.
31. Whiteway, M. and Szostak, J.W. (1985) The ARD1 gene of yeast functions in the switch between the mitotic cell cycle and alternative developmental pathways. *Cell*, **43**, 483–492.
32. Wang, Y., Mijares, M., Gall, M.D., Turan, T., Javier, A., Bornemann, D.J., Manage, K. and Warrior, R. (2010) Drosophila variable nurse cells encodes arrest defective 1 (ARD1), the catalytic subunit of the major N-terminal acetyltransferase complex. *Dev. Dyn.*, **239**, 2813–2827.
33. Ingram, A.K., Cross, G.A.M. and Horn, D. (2000) Genetic manipulation indicates that ARD1 is an essential Nα-acetyltransferase in Trypanosoma brucei. *Mol. Biochem. Parasitol.*, **111**, 309–317.
34. Sonnichsen, B., Koski, L.B., Walsh, A., Marschall, P., Neumann, B., Brehm, M., Alleaume, A.M., Artelt, J., Bettencourt, P., Cassin, E. *et al.* (2005) Full-genome RNAi profiling of early embryogenesis in Caenorhabditis elegans. *Nature*, **434**, 462–469.
35. Kalvik, T.V. and Arnesen, T. (2013) Protein N-terminal acetyltransferases in cancer. *Oncogene*, **32**, 269–276.

36. Rope, A.F., Wang, K., Evjenth, R., Xing, J., Johnston, J.J., Swensen, J.J., Johnson, W.E., Moore, B., Huff, C.D., Bird, L.M. *et al.* (2011) Using VAAST to identify an X-linked disorder resulting in lethality in male infants due to N-terminal acetyltransferase deficiency. *Am. J. Hum. Genet.*, **89**, 28–43.
37. Van Damme, P., Stove, S.I., Glomnes, N., Gevaert, K. and Arnesen, T. (2014) A Saccharomyces cerevisiae model reveals in vivo functional impairment of the Ogden syndrome N-terminal acetyltransferase NAA10 Ser37Pro mutant. *Mol. Cell. Proteomics*, **13**, 2031–2041.
38. Zaidi, S., Choi, M., Wakimoto, H., Ma, L., Jiang, J., Overton, J.D., Romano-Adesman, A., Bjornson, R.D., Breitbart, R.E., Brown, K.K. *et al.* (2013) De novo mutations in histone-modifying genes in congenital heart disease. *Nature*, **498**, 220–223.
39. Esmailpour, T., Riazifar, H., Liu, L., Donkervoort, S., Huang, V.H., Madaan, S., Shoucri, B.M., Busch, A., Wu, J., Towbin, A. *et al.* (2014) A splice donor mutation in NAA10 results in the dysregulation of the retinoic acid signalling pathway and causes Lenz microphthalmia syndrome. *J. Med. Genet.*, **51**, 185–196.
40. Popp, B., Stove, S.I., Endele, S., Myklebust, L.M., Hoyer, J., Sticht, H., Azzarello-Burri, S., Rauch, A., Arnesen, T. and Reis, A. (2014) De novo missense mutations in the NAA10 gene cause severe non-syndromic developmental delay in males and females. *Eur. J. Hum. Genet.*, doi: 10.1038/ejhg.2014.150.
41. Grauffel, C., Abboud, A., Liszczak, G., Marmorstein, R., Arnesen, T. and Reuter, N. (2012) Specificity and versatility of substrate binding sites in four catalytic domains of human N-terminal acetyltransferases. *PLoS ONE*, **7**, e52642.
42. Lee, J.T. and Bartolomei, M.S. (2013) X-inactivation, imprinting, and long noncoding RNAs in health and disease. *Cell*, **152**, 1308–1323.
43. Lyon, M.F. (1961) Gene action in the X-chromosome of the mouse (Mus musculus L.). *Nature*, **190**, 372–373.
44. Bolduc, V., Chagnon, P., Provost, S., Dubé, M.P., Belisle, C., Gingras, M., Mollica, L. and Busque, L. (2008) No evidence that skewing of X chromosome inactivation patterns is transmitted to offspring in humans. *J. Clin. Invest.*, **118**, 333–341.
45. Sado, T. and Sakaguchi, T. (2013) Species-specific differences in X chromosome inactivation in mammals. *Reproduction*, **146**, R131–R139.
46. Lee, K., Choi, K. and Ouellette, M. (2004) Use of exogenous hTERT to immortalize primary human cells. *Cytotechnology*, **45**, 33–38.
47. Ouellette, M.M., McDaniel, L.D., Wright, W.E., Shay, J.W. and Schultz, R.A. (2000) The establishment of telomerase-immortalized cell lines representing human chromosome instability syndromes. *Hum. Mol. Genet.*, **9**, 403–411.
48. Du, W. and Pogoriler, J. (2006) Retinoblastoma family genes. *Oncogene*, **25**, 5190–5200.
49. Nevins, J.R. (2001) The Rb/E2F pathway and cancer. *Hum. Mol. Genet.*, **10**, 699–703.
50. Manning, A.L. and Dyson, N.J. (2011) pRB, a tumor suppressor with a stabilizing presence. *Trends Cell Biol.*, **21**, 433–441.
51. Shin, D.H., Chun, Y.-S., Lee, K.-H., Shin, H.-W. and Park, J.-W. (2009) Arrest defective-1 controls tumor cell behavior by acetylating myosin light chain kinase. *PLoS ONE*, **4**, e7451.
52. Gromyko, D., Arnesen, T., Ryningen, A., Varhaug, J.E. and Lillehaug, J.R. (2010) Depletion of the human Nα-terminal acetyltransferase A induces p53-dependent apoptosis and p53-independent growth inhibition. *Int. J. Cancer*, **127**, 2777–2789.
53. Kuo, H.-P., Lee, D.-F., Chen, C.-T., Liu, M., Chou, C.-K., Lee, H.-J., Du, Y., Xie, X., Wei, Y., Xia, W. *et al.* (2010) ARD1 stabilization of TSC2 suppresses tumorigenesis through the mTOR signaling pathway. *Sci. Signal.*, **3**, ra9.
54. Hua, K.T., Tan, C.T., Johansson, G., Lee, J.M., Yang, P.W., Lu, H.Y., Chen, C.K., Su, J.L., Chen, P.B., Wu, Y.L. *et al.* (2011) N-alpha-acetyltransferase 10 protein suppresses cancer cell metastasis by binding PIX proteins and inhibiting Cdc42/Rac1 activity. *Cancer Cell*, **19**, 218–231.
55. Lim, J.-H., Park, J.-W. and Chun, Y.-S. (2006) Human arrest defective 1 acetylates and activates β-catenin, promoting lung cancer cell proliferation. *Cancer Res.*, **66**, 10677–10682.
56. Van Damme, P., Lasa, M., Polevoda, B., Gazquez, C., Elosegui-Artola, A., Kim, D.S., De Juan-Pardo, E., Demeyer, K., Hole, K., Larrea, E. *et al.* (2012) N-terminal acetylome analyses and functional insights of the N-terminal acetyltransferase NatB. *Proc. Natl. Acad. Sci. USA*, **109**, 12449–12454.
57. Van Damme, P., Van Damme, J., Demol, H., Staes, A., Vandekerckhove, J. and Gevaert, K. (2009) A review of COFRADIC techniques targeting protein N-terminal acetylation. *BMC Proc.*, **3**, S6.
58. Van Damme, P., Gawron, D., Van Criekinge, W. and Menschaert, G. (2014) N-terminal proteomics and ribosome profiling provide a comprehensive view of the alternative translation initiation landscape in mice and men. *Mol. Cell. Proteomics*, **13**, 1245–1261.
59. Menschaert, G., Van Criekinge, W., Notelaers, T., Koch, A., Crappé, J., Gevaert, K. and Van Damme, P. (2013) Deep proteome coverage based on ribosome profiling aids mass spectrometry-based protein and peptide discovery and provides evidence of alternative translation products and near-cognate translation initiation events. *Mol. Cell. Proteomics*, **12**, 1780–1790.
60. Van Damme, P., Arnesen, T. and Gevaert, K. (2011) Protein alpha-N-acetylation studied by N-terminomics. *FEBS J.*, **278**, 3822–3834.
61. MacKerell, A.D., Bashford, D., Bellott, M., Dunbrack, R.L., Evanseck, J.D., Field, M.J., Fischer, S., Gao, J., Guo, H., Ha, S. *et al.* (1998) All-atom empirical potential for molecular modeling and dynamics studies of proteins. *J. Phys. Chem. B*, **102**, 3586–3616.
62. Van Damme, P., Arnesen, T., Ruttens, B. and Gevaert, K. (2013) In-gel N-acetylation for the quantification of the degree of protein in vivo N-terminal acetylation. *Methods Mol. Biol.*, **981**, 115–126.
63. Bell, P.B. Jr. (1978) Contact inhibition of movements in transformed and nontransformed cells. *Birth Defects Orig. Artic Ser.*, **14**, 177–194.
64. Fujito, T., Ikeda, W., Kakunaga, S., Minami, Y., Kajita, M., Sakamoto, Y., Monden, M. and Takai, Y. (2005) Inhibition of cell movement and proliferation by cell-cell contact-induced interaction of Necl-5 with nectin-3. *J. Cell. Biol.*, **171**, 165–173.
65. Weijer, C.J. (2009) Collective cell migration in development. *J. Cell. Sci.*, **122**, 3215–3223.
66. Arnesen, T., Gromyko, D., Horvli, O., Fluge, O., Lillehaug, J. and Varhaug, J.E. (2005) Expression of N-acetyl transferase human and human arrest defective 1 proteins in thyroid neoplasms. *Thyroid*, **15**, 1131–1136.
67. Masuda, S., Das, R., Cheng, H., Hurt, E., Dorman, N. and Reed, R. (2005) Recruitment of the human TREX complex to mRNA during splicing. *Genes Dev.*, **19**, 1512–1517.
68. Folco, E.G., Lee, C.S., Dufu, K., Yamazaki, T. and Reed, R. (2012) The proteins PDIP3 and ZC11A associate with the human TREX complex in an ATP-dependent manner and function in mRNA export. *PLoS ONE*, **7**, e43804.
69. Eswar, N., Webb, B., Marti-Renom, M.A., Madhusudhan, M.S., Eramian, D., Shen, M.-Y., Pieper, U. and Sali, A. (2007),

Comparative protein structure modeling using MODELLER. *Curr. Protoc. Protein Sci.*, chapter 2, Unit 2.9.

70. Phillips, J.C., Braun, R., Wang, W., Gumbart, J., Tajkhorshid, E., Villa, E., Chipot, C., Skeel, R.D., Kalé, L. and Schulten, K. (2005) Scalable molecular dynamics with NAMD. *J. Comput. Chem.*, **26**, 1781–1802.
71. Kollman, P.A., Massova, I., Reyes, C., Kuhn, B., Huo, S., Chong, L., Lee, M., Lee, T., Duan, Y., Wang, W. *et al.* (2000) Calculating structures and free energies of complex molecules: combining molecular mechanics and continuum models. *Acc. Chem. Res.*, **33**, 889–897.
72. Davis, M.E., Madura, J.D., Luty, B.A. and McCammon, J.A. (1991) Electrostatics and diffusion of molecules in solution – simulations with the University of Houston Brownian Dynamics program. *Comput. Phys. Commun.*, **62**, 187–197.
73. Allen, R.C., Zoghbi, H.Y., Moseley, A.B., Rosenblatt, H.M. and Belmont, J.W. (1992) Methylation of HpaII and HhaI sites near the polymorphic CAG repeat in the human androgen-receptor gene correlates with X chromosome inactivation. *Am. J. Hum. Genet.*, **51**, 1229–1239.
74. Staes, A., Impens, F., Van Damme, P., Ruttens, B., Goethals, M., Demol, H., Timmerman, E., Vandekerckhove, J. and Gevaert, K. (2011) Selecting protein N-terminal peptides by combined fractional diagonal chromatography. *Nat. Protocols*, **6**, 1130–1141.
75. Helsens, K., Colaert, N., Barsnes, H., Muth, T., Flikka, K., Staes, A., Timmerman, E., Wortelkamp, S., Sickmann, A., Vandekerckhove, J. *et al.* (2010) ms_lims, a simple yet powerful open source laboratory information management system for MS-driven proteomics. *PROTEOMICS*, **10**, 1261–1264.